AN INVESTIGATION OF THE ABSORPTION OF LEAD (PB) THROUGH SKIN WITH HAIR USING SYNCHROTRON X-RAY TECHNIQUES

AN INVESTIGATION OF THE ABSORPTION OF LEAD (PB) THROUGH SKIN WITH HAIR USING SYNCHROTRON X-RAY TECHNIQUES

By HELEN MELINO, B.Sc.

A Thesis Submitted to the Radiation Sciences Program and School of Graduate Studies in Partial Fulfilment of the Requirements for the Degree Master of Science

McMaster University Hamilton, Ontario
MASTER OF SCIENCE (2025) (Radiation Sciences)

TITLE: An Investigation of the Absorption of Lead (Pb) through Skin with Hair using Synchrotron X-ray Techniques

AUTHOR: Helen Melino,
B.Sc. Honours Medical Physics
(Toronto Metropolitan University)

SUPERVISORS: Dr. Fiona McNeill
Dr. Michael Farquharson

COMMITTEE: Dr. Bruce Wainmann
Dr. Viorica F Bondici

NUMBER OF PAGES: xvi, 100

Lay abstract

Lead is a toxic substance and can cause severe health issues at low levels of exposure. Recognized pathways of lead intake include ingestion and inhalation, while the pathway of absorption through the skin is not well understood and often ignored. This thesis aims to investigate the skin absorption pathway of lead, particularly for skin with hair. Previous research in our group showed evidence of lead accumulation within skin structures which may be directly related to the presence of hair follicles. The hypothesis behind this thesis is that substances applied to the skin surface may be absorbed more easily by entering sweat glands and hair follicles. Traditional diffusion experiments where lead was applied to skin, followed by synchrotron micro x-ray imaging of lead-exposed skin samples show that lead is easily absorbed into the skin following application, and that contrary to the hypothesis, there is no evidence that hair increases the absorption.

Abstract

The acknowledged pathways of lead entry to the body include ingestion and inhalation, with absorption rarely cited as a large contributor to body lead burden. This thesis investigates the absorption of lead into skin with hair using both traditional passive diffusion experiments and synchrotron x-ray imaging techniques. Pig skin with hair was used as the test membrane in a Franz diffusion cell set-up. A solution of lead (II) acetate dissolved in deionized water was applied to the skin surface and allowed to passively diffuse through the skin layers into a deionized water receptor solution. Diffusion times of 24, 48 and 72 hours were used to determine total lead content passing through the epidermis and dermis through inductively coupled plasma mass spectroscopy (ICP-MS) for the traditional diffusion analysis.

Additional diffusion times of 0.25, 0.5, 1, 2, or 24 hours were studied by synchrotron-based micro x-ray fluorescence (μXRF) and x-ray absorption spectroscopy (XAS) measurements. To our knowledge, this thesis presents the first μXRF images of the elemental distribution of lead in hairy skin following cutaneous application.

ICP-MS results show that the diffusion of lead through hairy skin is impeded by the accessory skin structures, resulting in lower lead content in the receptor solution following diffusion through hairy skin compared to hairless skin. μXRF results show the progression of lead diffusion through the skin over time, accumulation of lead in epidermal cells, and significant differences in the depth and intensity of lead diffusion through the skin with respect to the position of the hair underlying the skin surface ($p < 0.0125$).

XAS results show that the Pb^{2+} ion from the applied lead (II) acetate interacts with subcutaneous components and structures to form different compounds, often $PbCO_3$ and $PbCl_2$, however more physiologically relevant reference compounds should be used for XAS studies in the future to more accurately identify lead compounds formed in skin.

Acknowledgements

I would like to express my sincere thanks and gratitude to my supervisors, Fiona McNeill and Michael Farquharson, for their confidence in me to pursue this project. They have given me so many opportunities to learn new lab techniques and for growth in my professional career, for which I am truly grateful. Fiona especially has created such a welcoming lab environment in the Toxic Allure lab which was a pleasure to work in. To my lab members (Lisa, Kirstin, Jayna, Dhara, Molly, Charlie, and Siya), thank you for helping me prepare my experiments, and for always bringing unique ideas and laughter into the lab. You all inspire me much more than you know.

I would also like to thank beamline scientists Ibi Bondici and Sebastian Schöder for their guidance and thoughtful suggestions on the analysis of synchrotron data. The time they spent to meet with me and answer my unending questions is truly appreciated. I am also very grateful for the help of Rina Green in the collection of hair samples from her salon in Vaughan. Her kindness and care with collection is greatly appreciated.

A thank you is also extended to Mary Jo Smith, Marcia Reid, and Mouhanad Babi, who were extremely helpful in sample preparation with a cryomicrotome, ultramicrotome, and educating me on the use of the polarized light microscope.

To my friends, thank you for helping my see the light at the end of the tunnel, and my fellow graduate students for making my time at McMaster memorable. I especially want to thank Melanie Lemaire for supporting me through the little wins in this project and in my career, and Chloe Green for helping me work through physics problems I encountered during my analysis.

Thank you to my family for their continual belief in me through my academic and career endeavours. I appreciate your love and support very much!

Table of Contents

List of Figures

List of Tables

List of Abbreviations and Symbols

ANKA Angströmquelle Karlsruhe

CALM Center for Advanced Light Microscopy

CCEM Canadian Centre for Electron Microscopy

CLS Canadian Light Source

DESY Deutsches Elektronen Synchrotron

ESRF European Synchrotron Radiation Facility

FDA Food and Drug Administration

HEPA High-Efficiency Particulate Air

H_2S hydrogen sulfide

ICP-MS Inductively coupled plasma mass spectrometry

ICRP International Commission on Radiological Protection

K_p permeability coefficient

LCF linear combination fitting

μ(E) Energy absorption coefficient

μXRF micro x-ray fluorescence

NIST National Institute for Standards and Technology

OECD Organisation for Economic Co-operation and Development

Pb lead

$Pb(CH_3COO)_2 \cdot 3H_2O$ lead (II) acetate trihydrate

$PbCl_2$ lead (II) chloride

$PbCO_3$ lead (II) carbonate

PbO lead (IV) monoxide

PbO_2 lead (IV) dioxide

Pb_3O_4 lead (IV) tetroxide

$Pb_3(PO_4)_2$ lead (II) phosphate

ppb parts per billion

PPD *p*-phenylenediamine

ppm parts per million

PbS lead (II) sulfide

$PbSO_4$ lead (II) sulfate

PUMA Photons used for Ancient Materials

SC stratum corneum

SDD silicon drift detector

SSRL Stanford Synchrotron Radiation Lightsource

XANES x-ray absorption near edge structure

XAS x-ray absorption spectroscopy

XRF x-ray fluorescence

Declaration of Academic Achievement

I declare that this thesis is my own original work and that I am the sole author. I have read through the thesis and ensured it does not include any plagiarism.

1 Introduction

1.1 Historical Context and Motivation

Lead is a ubiquitous and toxic element that has been used in many materials including batteries, paints, piping, pesticides, hair dyes and historical cosmetics [1, 2]. Lead within the body can have detrimental effects on various bodily systems including the central nervous system, endocrine system, and reproductive system [2-5]. Any level of lead in the body is considered unsafe, but an adult blood lead level of 70 μg/dL or greater is considered clinical lead poisoning [6]. Lead exposure is often attributed to the pathways of ingestion and inhalation [4]. Since it is difficult to observe lead exposure from skin absorption *in vivo* using conventional blood and urine screening, the contributions of this pathway may have been greatly underestimated [7]. In a study on the absorption of inorganic lead nitrate, Lilley et al. have observed that after cutaneous lead application, accumulation of lead in the body was found in the sweat glands at distant locations from the initial lead application, however there was no lead observed in the blood or urine of the human volunteers [4]. It has also been found that organic lead compounds can permeate the skin, while inorganic lead compounds are said to provide minimal contribution to body lead burden [4, 8].

Historically, inorganic lead compounds, namely lead acetate or lead carbonate, were dissolved in various solutions that were applied to the face to improve the texture and colour of the skin, as well as to hide blemishes [9]. The lightness of the face was associated with social status in the eighteenth century, but the use of these lead-containing cosmetics was also linked to multiple reports of lead poisoning, one of the famous cases being the lead

poisoning and eventual death of the Countess of Coventry [9, 10]. Despite current assumptions regarding the absorption of lead through the skin, cases of lead poisoning linked to the use of lead-containing cosmetics suggest that the threat posed by continuous application of lead compounds to the skin is not negligible. Currently, the FDA has placed a limit on lead content in cosmetics at 10 ppm [11].

Like facial make-up, hair dyes have been used through history to differentiate social status [12]. The use of lead acetate as a colourant in hair dye formulations was banned as recently at 2008 in Canada and 2022 in the United States after the FDA ruled there was not a "reasonable certainty of no harm" from its incorporation in progressive hair dyes based on available data [13]. In hair dyes, longer dye persistence is associated with diffusion of the colourant molecules into the hair cortex, with the established diffusion path of the colourant molecule including passage through non-keratinized regions of the endocuticle towards keratinized regions, with subsequent incorporation into the hair matrix [12]. Although there is not much evidence of harm posed by applying lead compounds to hair on the head, the hair follicle is vascularized and thus may provide a pathway to the circulatory system.

One of the existing hypotheses for the predominant mechanism of percutaneous absorption assumes that substances applied to the skin may enter the skin through hair follicles, and sebaceous and/or sweat glands [2, 7, 14, 15]. However, the underlying mechanism of lead absorption into the skin or hair follicles is not well understood. To gain a deeper understanding of the path of lead through the skin and hair, traditional diffusion

techniques and subsequent micro x-ray imaging can be used to both visualize and quantify this phenomenon.

1.2 Skin

The skin has a primary function of acting as a protective barrier to the external environment [16]. The skin consists of various layers, each with their own features and functions. The outermost and relatively impermeable layer is called the epidermis [16]. The epidermis is composed of four sublayers in thin skin or five sublayers in thick skin (found only on the palms and soles of feet) and is non-vascularized [17]. The most superficial layer of the epidermis, the stratum corneum (SC), is often referred to as the rate-limiting layer of the skin membrane as it is primarily composed of tightly interconnected keratinocytes, causing limited permeability of the skin to foreign substances [17-19]. Subsequent layers of the epidermis of thin skin, listed from superficial to most deep, include the stratum granulosum, stratum spinosum and stratum basale, which have functions of producing large amounts of keratin, immune response, and anchoring the epidermis to the dermis, respectively [17]. Deep to the epidermis is the dermis, which includes features such as blood and lymph vasculature and nerve fibers [17]. Accessory structures, including hair follicles and sweat glands extend distally from the dermis [16, 17]. Beneath the dermis is the subcutaneous fat layer, containing adipocytes and a limited number of capillaries which helps position the skin relative to underlying tissues and organs [17].

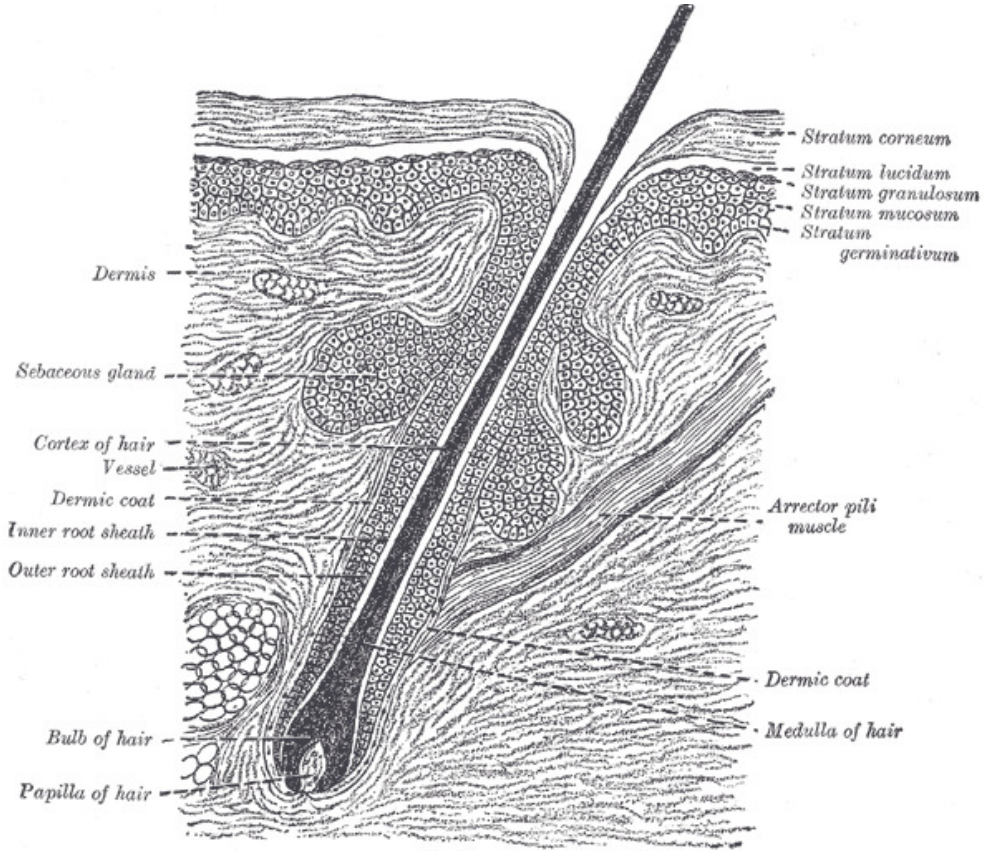

Figure 1.1: An illustration of a cross section of human skin showing the epidermis, dermis, hair follicle, and sebaceous glands [20].

Keratinocytes are the most abundant epithelial cells responsible for the structure and impermeability of the epidermis, secretion of keratin fibers, and storing melanin [17]. Keratins are abundant in cysteine residues and thus sulfhydryl groups, which most metals, including zinc, lead, cadmium, copper, silver, mercury and bismuth, have a high affinity for [21, 22]. Melanocytes produce two types of melanin, namely pheomelanin and eumelanin, responsible for either red-yellow or brown-black pigmentation, respectively [17]. Melanin is important for protection from UV radiation to the DNA in keratinocytes, responding to UV exposure by increasing their melanin production [17]. Additionally,

melanin pigments can bind cations such as Pb^{2+} at physiological pH since they contain negatively charged carboxyl groups [21]. Both keratin and melanin are incorporated into the hair matrix.

The percutaneous absorption of lead compounds has been previously studied through both *in vivo* and *in vitro* experiments [8, 23]. Results obtained from *in vivo* experiments performed on human volunteers have shown that inorganic lead compounds can be absorbed rapidly through the skin and transported around the body, however Lilley et al. were not able to detect significant increases in blood lead levels following the cutaneous application of lead nitrate or lead acetate [4, 7]. Although *in vitro* studies exist, they have not used been considered reliable as they often do not follow standard diffusion testing guidelines or have used the skin of animals, such as rats, known to overestimate the percutaneous absorption rate of human skin [2]. Because pigs have structural and physiological similarities to human skin, including similar epidermis, dermis and follicle structures, SC thickness and blood vessel density, pig skin has been suggested as the best surrogate for human skin for *in vitro* experiments [2, 24, 25]. The main difference between pig and human skin are the sweat glands, where most regions of human skin are populated with eccrine sweat glands, and the majority of porcine sweat glands are apocrine [17, 25]. Eccrine sweat glands open onto the surface of the skin and secrete sweat composed of mainly water and NaCl, while apocrine sweat glands are associated with hair follicles into which they secrete viscous, lipid-rich sweat containing proteins and sugars [17, 26]. In addition, sebaceous glands are present in the skin and are also associated with the hair follicle, secreting sebum, a viscous, lipid-rich substance containing components such as

triglycerides and cholesterol [17, 26]. Due to the hydrophilic nature of lead acetate, bodily secretions mainly composed of lipids, such as apocrine sweat and sebum, may impede the diffusion of lead into the skin.

While *in vivo* and *in vitro* studies provide evidence of percutaneous lead absorption, they are unable to describe the spatial distribution of lead in the skin as it is absorbed. Previous synchrotron micro x-ray fluorescence (μXRF) images acquired by our lab group at the Canadian Light Source (CLS) at the BioXAS-Imaging beamline in 2024 show evidence of lead accumulation in pig skin following a 48-hour lead diffusion experiment, with specific accumulation in amorphous structures beneath the epidermal layer of the skin. Through comparison with published histology of pig skin, these structures were determined to be sweat glands [25].

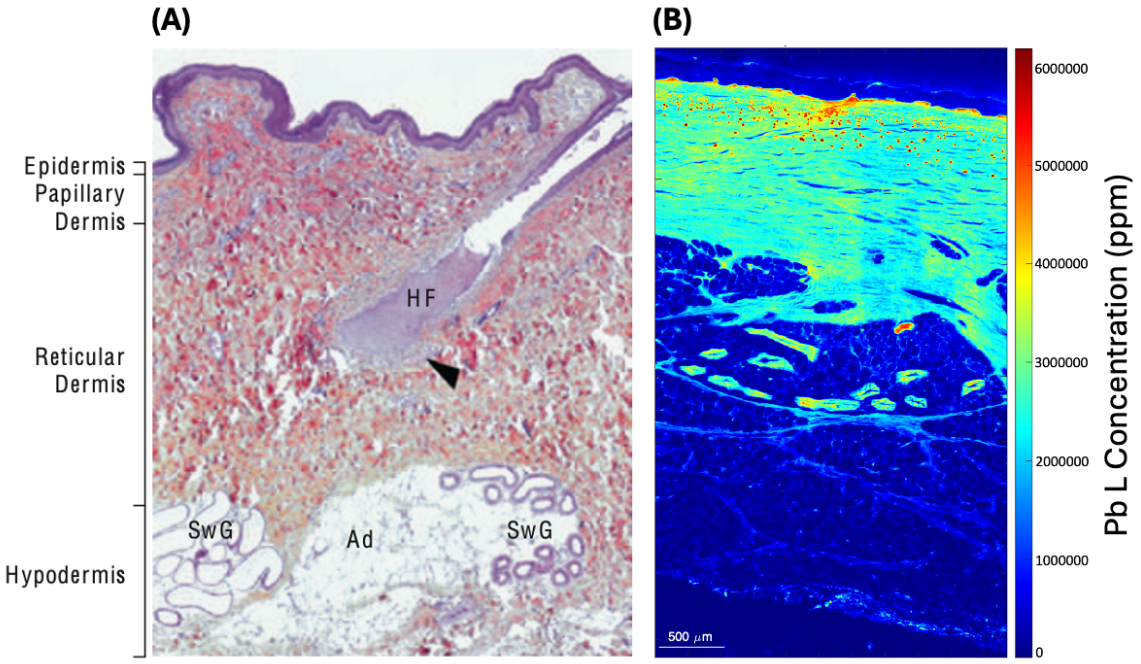

Figure 1.2: Comparison of (A) a haematoxylin-eosin-saffron slide depicting pig skin anatomy [25] to (B) results from synchrotron μXRF imaging of pig skin exposed to lead (II) acetate. μXRF imaging data was acquired in March 2024 at the BioXAS-Imaging beamline at the CLS using a beam energy of 13.45 keV with a step size of 5 μm and dwell time of 100 ms. Sweat glands appear as amorphous, ovular rings beneath the dermis in both images.

Evidence of lead accumulation in sweat glands, along with the knowledge that apocrine sweat glands and sebaceous glands branch off of the hair shaft in the dermal layer of the skin, have made an investigation of the effects of lead absorption through skin containing hair a key aim of this project.

1.3 Hair

Hair is mainly composed of keratin, melanin, and trace quantities of metallic elements, including mercury and lead [12, 17, 21, 27]. The hair consists of various layers, including the cuticle, cortex, and the medulla. The cuticle includes layers of overlapping scales covering the hair shaft in the longitudinal direction and contains an external thin membrane with cysteine residues responsible for the hydrophobic nature of the hair fiber [12, 27]. The cuticle is reported to contain three layers with decreasing cysteine content approaching the medulla [12]. The matrix of the hair, containing cells filled with keratin, is formed by the cortex [12]. The cuticle and cortical cells are linked by the cell membrane complex and is usually referred to as a non-keratinized region due a low presence of sulfur-containing amino acids [12, 28]. Non-keratinized regions have been reported as an important pathway for the diffusion of molecules into the inner layers of the hair shaft [12]. At the center of the hair shaft is the medulla, which is usually discontinuous or absent along the length of the hair shaft in humans and can be empty or filled with sponge keratin [12].

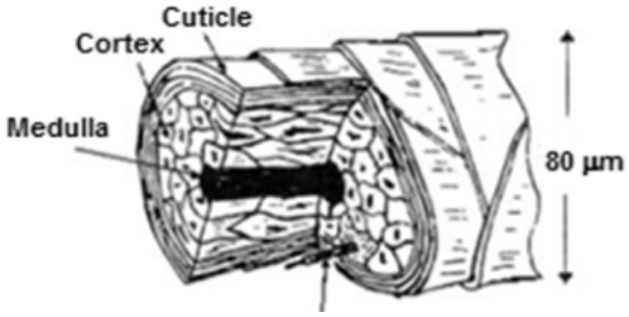

Figure 1.3: Morphology of a human hair shaft [21].

Human hair can be classified into three broad categories of either terminal, vellus, or intermediate hair, depending on appearance and origin [27, 29]. Terminal hairs are long, thick, often medullated, and usually extend more than 3 mm into the hypodermis [30]. Terminal hairs can be found on both androgen-independent body regions, including the eyebrows and eyelashes, and hormone-dependent body regions such as the scalp, beard, chest, and pubic regions [29, 30]. Contrastingly, vellus hairs are fine, short, non-medullated, and found on the areas of the body which are generally considered hairless [29]. Intermediate hairs are intermediate in length and thickness and can be found on the legs [29]. Pig hair is classified similarly to human hair, with general hair types including guard (bristle), awl, auchene, zigzag, tactile, and wool-like hair [31, 32]. As the most abundant pig hair type, guard hairs are straight, thick, and are longest on the middorsal area of the back [31, 32]. On average, the range of the midshaft diameter of middorsal guard hairs is 0.1-0.5 mm [32]. Awl hairs are also straight, but are thicker and more blunt than guard hairs, while both auchene and zigzag hairs are thin and characterized by either one or multiple oblique angle bends along the shaft [33]. Tactile or vibrissae hairs are found on the mental glands of pigs, while wool-like hair is only found in certain pig breeds, such as the Mangalica pig [31, 32]. In a study of the hair of Yorkshire pigs, guard, awl, auchene and zigzag hair types were all identified on the dorsal side of the pig, however Zou et al. note that guard hairs were most similar to human scalp hair [31]. Although pigs serve as a good surrogate for percutaneous absorption studies of human skin, human hair differs from other lower animals in various respects. Human hairs often carry a consistent and evenly distributed pigmentation along the length of the hair shaft, however colour changes along

short lengths of hair and higher pigment densities near the medulla can be observed for lower animals [27]. When present in humans, the medulla can have a width of less than one third of the hair shaft diameter, while lower animals tend to have a continuous, structured medulla which is greater than one third of the hair shaft diameter [27, 28].

Endogenous contamination of the hair occurs when exposure to substances results in their incorporation into the hair matrix during its growth, while exogenous contamination results from contact of the hair with substances in the external environment such as cosmetics, dust, and smoke [21]. Dyeing the hair often involves the use of an oxidizing agent along with a dye molecule, based on the historical observation of a colour compound produced by *p*-phenylenediamine (PPD) on various substrates when subjected to oxidation [34]. This oxidation also damages the cuticle, allowing the dye molecules to enter and stain the cortex and medulla [17]. Historical hair dyes using lead acetate as the dye molecule utilized the oxidation process, with the oxidation allowing the formation of insoluble lead sulfides in the hair [35]. Many metals, including lead, have a high affinity for the sulfhydryl groups found in keratin and therefore trace elements from dusts can easily attach to hair keratin and persist in the hair for long periods of time [21]. This persistence in the hair is aided by additional ionic bonding with melanin pigments [21]. Because of this binding affinity, human hair has been suggested for use as a biosorbent to eliminate heavy metal ions from aqueous solutions, with bleached and dyed hair showing a greater capacity for biosorption of heavy metal ions, including Pb^{2+}, than untreated human hair [36].

1.4 Diffusion Experiment Set-up

Substances applied to the skin surface can diffuse passively through the skin layers once they have passed through the stratum corneum. The rate of diffusion of substances through the skin can be studied through *in vitro* experiments, which usually employ the Franz cell diffusion apparatus [37].

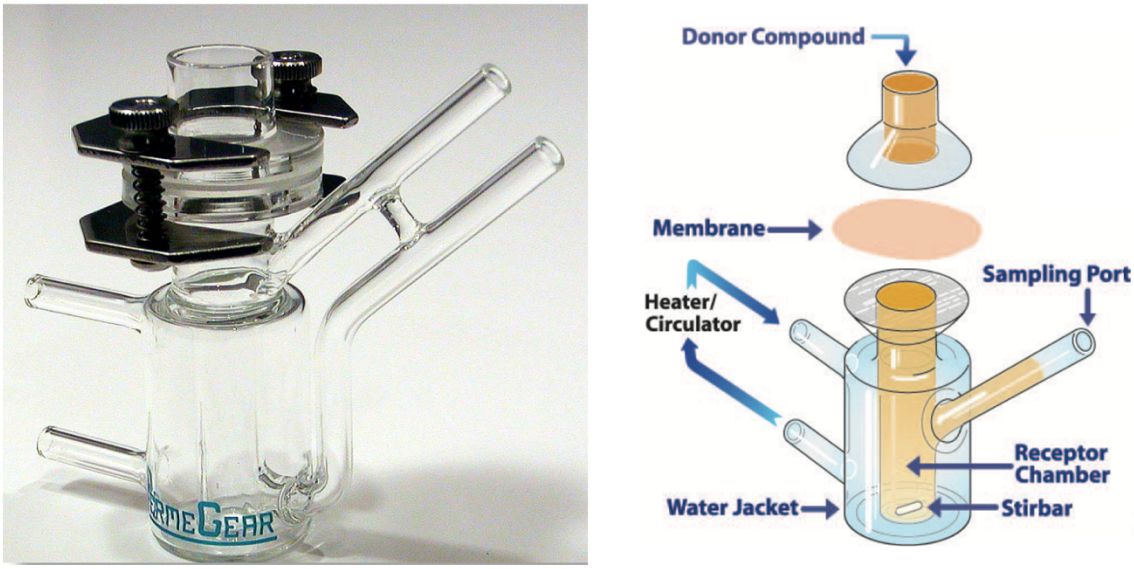

Figure 1.4: A photograph and diagram illustrating the main components of the Franz diffusion cell apparatus [38]. The membrane employed in this thesis work was trimmed pig skin.

The Franz diffusion cell set-up follows the OECD (Organisation for Economic Co-operation and Development) guidelines for *in vitro* transdermal pharmaceutical diffusion studies [39]. Each Franz cell is composed of a receptor chamber and a donor chamber cap [37]. The receptor chamber is surrounded by a water jacket through which heated water is circulated to maintain a physiological temperature of 37°C during diffusion. Before the

placement of the diffusion membrane, the receptor chamber is filled with a solution which should mimic physiological conditions but should not impede diffusion of the test solution [39]. After the membrane and donor chamber are positioned for diffusion, the test solution is applied through the donor vestibule to come into contact with the diffusion membrane and diffuse into the receptor chamber. The rate of the diffusion of the test solution through the test membrane is determined by sampling, analyzing, and replacing the receptor solution at various time intervals [38]. By collecting diffusion data for various time intervals, a diffusion curve can be constructed, which can be used to determine the permeability constant, K_p, a metric for describing the rate of penetration of a chemical through a membrane [2, 38, 40]. This quantity is essentially the slope of the linear portion of a diffusion curve describing the concentration detected in the receptor solution at various time intervals [38, 40]. Results from inductively coupled plasma mass spectrometry (ICP-MS) analysis applied to the diffusion data are used to determine the K_p, but this provides no spatial information for the diffusion of a test substance across a membrane. Synchrotron-based x-ray techniques can be used in combination with ICP-MS analysis to visualize the elemental distribution of the diffused donor solution components in the skin.

1.5 Inductively coupled plasma mass spectrometry (ICP-MS)

Inductively coupled plasma mass spectrometry (ICP-MS) is a technique commonly used for ultra-trace element determination at the ppm (μg/g) and ppb (ng/g) level [21]. This technique is element-specific and is sensitive enough to quantify the ultra-low levels of lead within the receptor solution following Franz cell diffusion. The results of this analysis

can be used to construct a diffusion curve to determine fundamental diffusion parameters of the skin membrane, including the K_p. ICP-MS analysis is not limited to receptor solution as it can also be applied to skin and hair samples for elemental determination, providing an average concentration of the element of interest within the sample since the skin and hair would be acid-digested prior to analysis. The ICP-MS results can be used as a comparison methodology to the spatially resolved elemental concentration determination resulting from element-specific imaging techniques, such as synchrotron-based x-ray fluorescence imaging.

1.6 Synchrotron Source

Synchrotron-based techniques are powerful tools for non-invasive quantification of materials. In a synchrotron source, electrons originating from a linear accelerator are accelerated under vacuum conditions into a booster ring where they are further accelerated to reach an energy of approximately 1-8 GeV, and are then injected into the storage ring [41]. The storage ring is shaped like a polygon and constructed by bending magnets at the corners of the ring to connect the straight sections of the ring. Insertion devices such as wigglers or undulators can be incorporated into the straight sections of the storage ring to work along with bending magnets to produce the radiation source for beamlines [41]. Synchrotron x-ray radiation is produced by deflecting the electrons along their path to emit radiation in the forward direction. Beamlines are composed of x-ray mirrors and a monochromator, which allows collimation, selection of the energy of interest and focusing to micro- or nano-scale resolutions [41, 42]. Synchrotron facilities are dispersed across the

world, with one facility in Canada, namely the Canadian Light Source (CLS) located in Saskatchewan. The data for this project was mainly collected at Synchrotron Soleil in France.

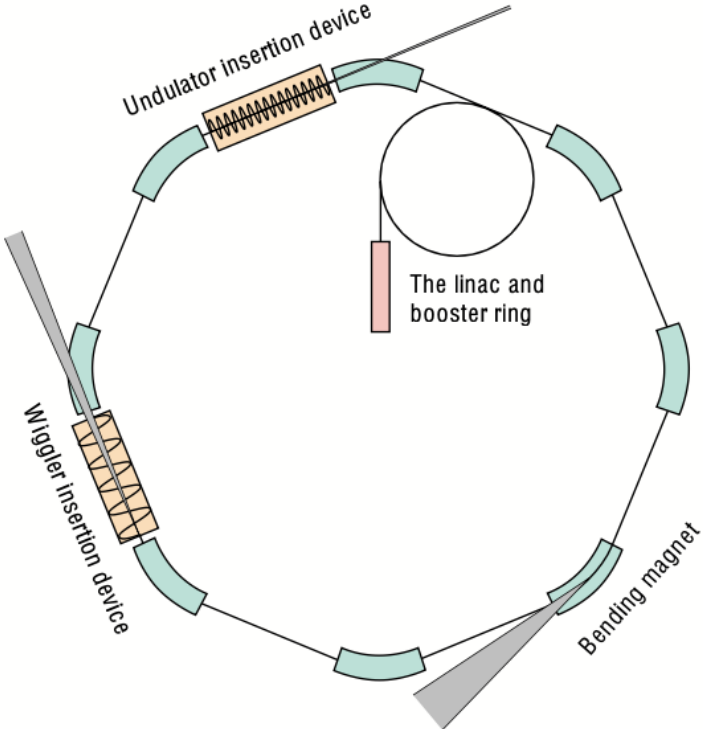

Figure 1.5: Schematic of a synchrotron and its components. Beamlines are tangential to the bending magnet, or parallel to the straight sections containing insertion devices [41].

The advantages of using synchrotron radiation instead of easily accessible x-ray devices include the ability to precisely tune the beam energy, the ability to achieve high intensity beams, and the tight collimation of the beam resulting in high resolution data acquisition,

all of which are required for x-ray fluorescence (XRF) imaging and x-ray absorption spectroscopy (XAS) of tissue sections [43].

1.6.1 X-ray Fluorescence (XRF) Imaging

X-ray fluorescence (XRF) is an elemental analysis technique which relies on the photoelectric effect [44]. If an incoming x-ray photon interacts with an inner shell electron with binding energy equal to or less than the incoming photon energy, that electron will be ejected, creating a vacancy and leaving the atom in an unstable excited state. To return to its ground state, an outer shell electron may transition down to fill the vacancy, emitting a photon with energy equal to the energy difference between its beginning and end states. This energy is characteristic to the specific transition, and is thus characteristic of the element. Auger electron emission is a competing process to the emission of a photon, with a probability of fluorescent emission of about 34% for the lead L3 transitions [45]. Because XRF is element-specific, this technique allows the mapping of elemental spatial distributions within biological samples, with synchrotron-based micro-XRF (μXRF) imaging allowing the distributions to be visualized at micron-level resolution [6].

μXRF imaging has been applied to various tissues to measure trace elements and biomarkers, including iron, copper, phosphorus and zinc [46-48]. μXRF imaging has also been used to display the elemental distribution of zinc in *Daphnia magna* after aquatic zinc exposure (figure 1.6), distribution of sulfur in bovine corneal tissue (figure 1.7), and distributions of calcium, copper, zinc and iron in human skin samples (figure 1.8) [49-51].

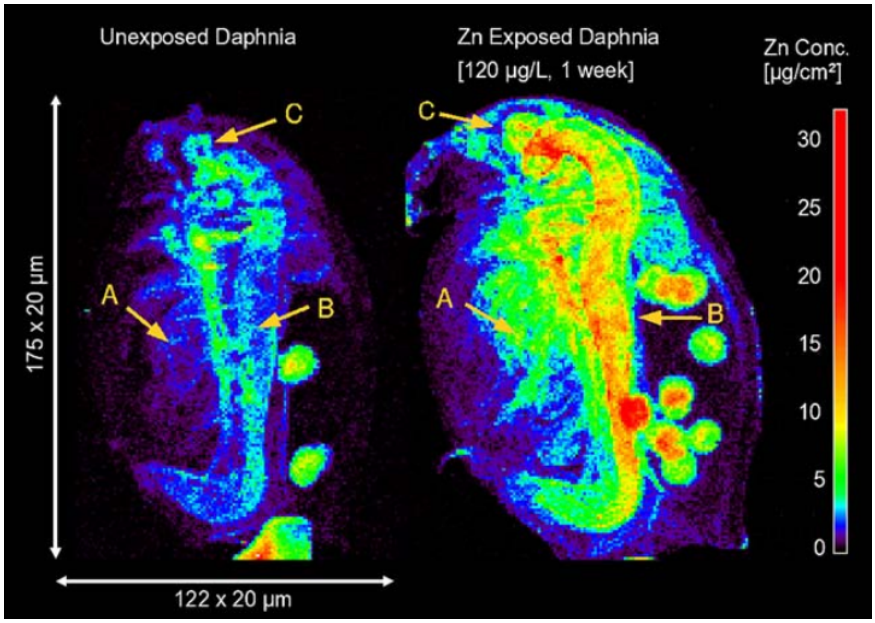

Figure 1.6: Distribution of zinc in aquatic organism, *Daphnia magna*, following aquatic zinc exposure imaged with µXRF at the synchrotron DESY [49].

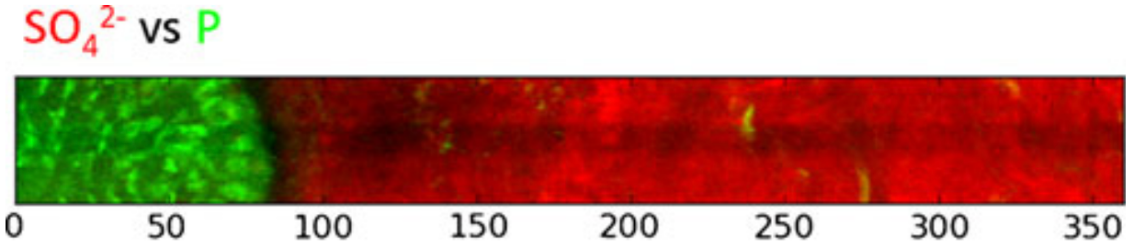

Figure 1.7: Distribution of sulfur (red) and phosphorus (green) in a bovine cornea sample imaged with µXRF at the ESRF [50].

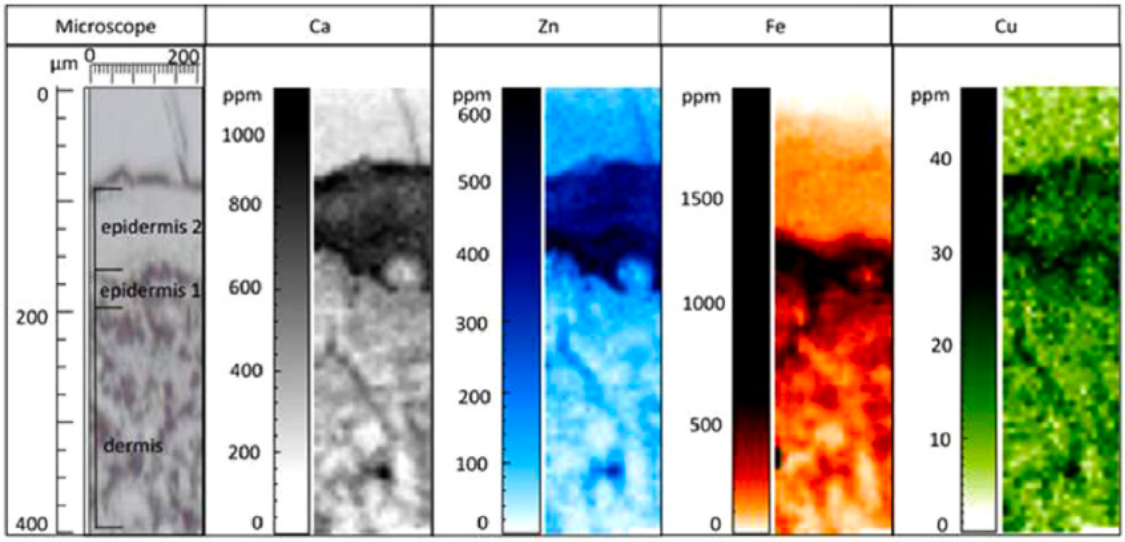

Figure 1.8: Distributions of calcium, copper, zinc and iron in a skin sample from a human foot imaged with µXRF at the ANKA synchrotron [51].

To our knowledge, synchrotron-based µXRF has not been applied to study the distribution of lead absorption in the skin.

1.6.2 X-ray Absorption Spectroscopy (XAS)

X-ray absorption spectroscopy (XAS) is a powerful technique for determining the chemical speciation and chemical bonding of a specific element in a sample with no or minimal sample preparation [52]. In this technique, energy is scanned near the x-ray absorption edge of the given metal, resulting in the excitation of core electrons to an empty higher energy state at beam energies equal to or above the electron binding energy [53-55]. Since XAS spectra measure the x-ray absorption as a function of beam energy, µ(E), a sharp increase in absorption is observed when the beam energy is near the binding energy of the

probed core shell electron [56]. This feature of the XAS spectrum is called the absorption edge.

Within a few eV of the edge energy lies the x-ray absorption near edge structure (XANES) region, where edge behaviour can be used to determine the oxidation states of absorbing atoms and local atomic environments by comparisons to reference spectra [53]. In addition to edge position, pre- and near-edge features are related to the chemical bonding of different compounds, and thus XANES can give an idea of the compounds present within a sample [55]. It is useful to view XANES as $\mu(E)$ versus E, as well as its first derivative since the inflection point corresponds to the exact value of the absorption edge of the probed compound [55].

While XAS of metal K-edges is possible for metals with low K-edge energies (<50 keV), it results in poor resolution in the XANES region from the short lifetime of the 1s core holes produced by the excited 1s electrons [42]. Metal L-edge XAS excites the 2p core electron, which is associated with intense transitions that are useful for determination of local structure [42, 53]. The lead L_3-edge includes the excitation of the 2p core electron to an s or d final state with probability described by Fermi's Golden Rule, creating an element-specific core-hole corresponding to the core electron binding energy [54, 57].

XANES are usually measured for materials science applications, however XANES have also been measured in biological samples, such as human bones, following an XRF line scan for sample orientation [58].

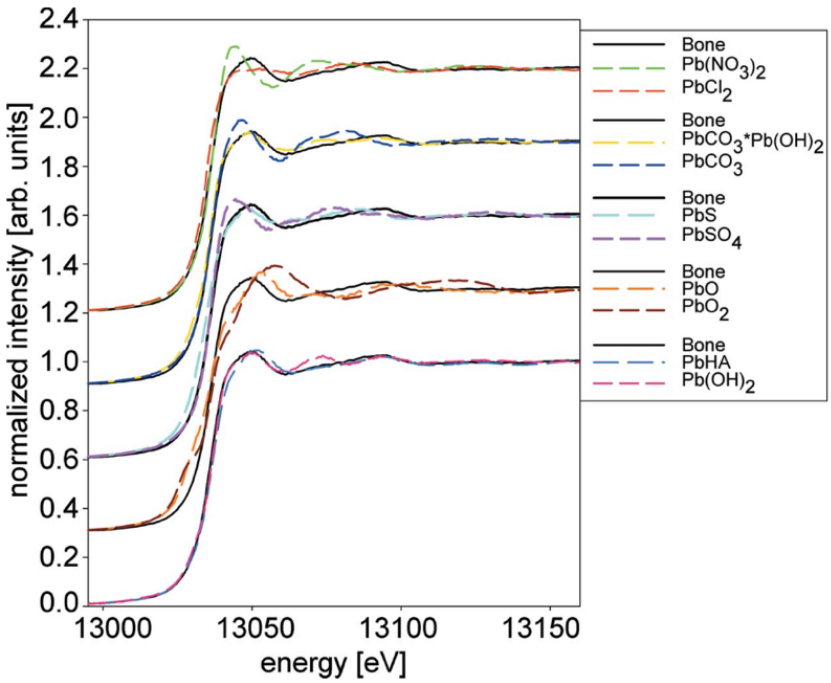

Figure 1.9: XANES spectra for bone samples compared to the XANES spectra for various reference lead compounds measured near the lead L_3-edge energy [58].

To our knowledge, XANES have not been collected for the chemical speciation of lead absorption in skin.

1.7 Project Objectives

This project aims to show the path of lead diffusion through skin when hair is present using synchrotron-based μXRF imaging, and to determine whether the lead acetate applied to the skin surface changes form as it travels through the skin through synchrotron-based XAS measurements. In addition, this project aims to determine the feasibility of using synchrotron-based μXRF to image the path of lead into the hair shaft when it is

externally applied. This work will be helpful in showing the pathways by which lead is absorbed by the skin, and could provide scientific evidence for policy decisions regarding the exclusion or not of lead acetate from hair-colouring products.

2 Methods

2.1 Preparation of Lead Compounds

In a ventilated dust hood, crystals of lead (II) acetate trihydrate ($Pb(CH_3COO)_2 \cdot 3H_2O$) were crushed and weighed into a polyethylene vial known to be free of lead. An appropriate volume of deionized water was added to achieve the desired concentration of lead acetate. The lead crystals were dissolved by physical agitation and inversion.

A lead acetate concentration of 0.33 g/mL (330000 ppm) was chosen for the Franz cell skin diffusion experiments as it is comparable to the lead concentrations of historical lead-based makeup according to the available literature where lead compounds were directly applied to the skin [59]. Lead solutions were prepared with a 25% (w/w) (250000 ppm) concentration for free-hair studies as the available literature noted concentrations of lead acetate in hair dyes which were equal to or less than 25% (w/w) [60]. Solutions were prepared within 7 days prior to their respective experiment to avoid evaporation.

2.2 Skin Experiments

2.2.1 Franz Cell Set-Up

Thick slabs of pig skin with dark, coarse hair protruding from the skin surface were obtained from a local butcher shop. The skin was cut with a scalpel into circular sections with a diameter of approximately 3 cm. The condition of the epidermal layer of the skin,

such as blemishes and presence of hair, was noted for each circular sample. The skin thickness was cut to either 2 mm to mimic a traditional diffusion study through the epidermis and dermis, or 4 mm to study the diffusion through the epidermis, dermis and into the subcutaneous fat layer. Skin was prepared for immediate use or stored in the fridge (4°C) for up to 7 days following purchase.

Figure 2.1: A slab of pig skin with dark hair. Pig hair is scarce and coarse, allowing the effects of a single hair on diffusion to be studied.

Franz cell diffusion experiments were conducted in a HEPA-filtered biosafety cabinet located in a HEPA-filtered clean room to avoid contamination of the experiments with lead particulates in dust. Average lead levels in Canadian house dust have been measured by Rasmussen et al. and reported as approximately 60 µg of lead per gram of house dust [61]. Ramussen et al. also showed evidence that some buildings built before 1980 can have lead levels of approximately 450 µg of lead per gram of house dust with some anomalous particulate reaching levels above 1700 µg of lead per gram of house dust

[61]. Franz cell measurements from our laboratory can result in lead concentrations in the parts per million or parts per billion range, so small levels of dust could be problematic, thus a HEPA-filtered clean room is essential for this work.

In the Franz cell set-up, the receptor chambers were filled with deionized water to ensure the diffusion was not impeded by the formation of insoluble lead compounds (e.g. $PbCl_2$) with the receptor solution at the skin-receptor interface. Each circular skin section was positioned on a receptor chamber with the epidermal side facing the donor compartment. The area of interest on the epidermal surface was centered to the 9 mm wide opening of the receptor chamber. The donor compartment cap was positioned directly on top of the skin so that the opening of the donor compartment was aligned with the area of interest on the skin. The donor cap and the skin were clamped to the receptor chamber to prohibit movement during diffusion.

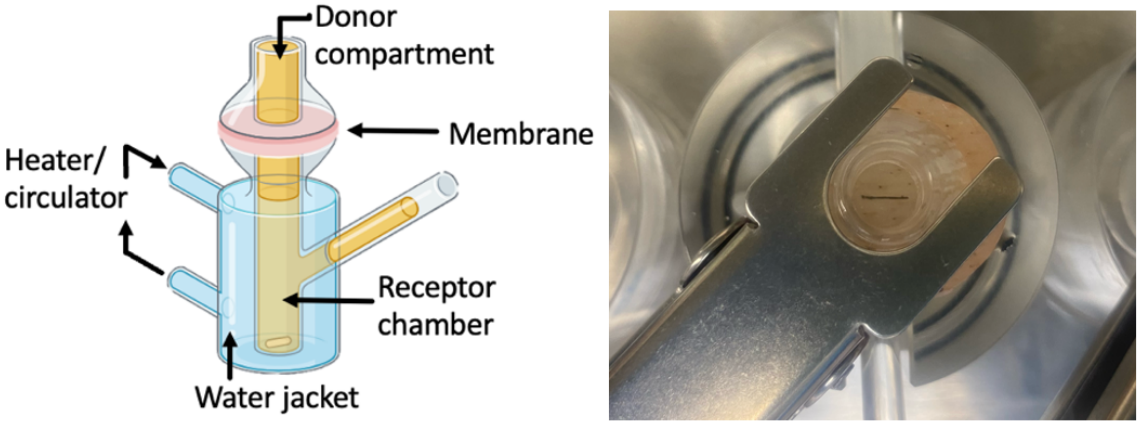

Figure 2.2: Franz diffusion cell components (left); a bird's eye view of the skin prior to lead application (right). Skin is positioned such that the hair (the black line at the center of the image) is aligned with the donor and receptor chamber openings.

Each experiment allowed for up to six samples to be considered, thus six samples were included for each diffusion time. For the hairy skin experiments, four of the six samples were prepared to study the diffusion of a single hair, one was prepared to study the diffusion of multiple hairs, and one was prepared to study the diffusion through skin with a high density of follicles visible through the stratum corneum. The data discussed in this thesis reflects the diffusion for samples which were prepared with a single protruding hair.

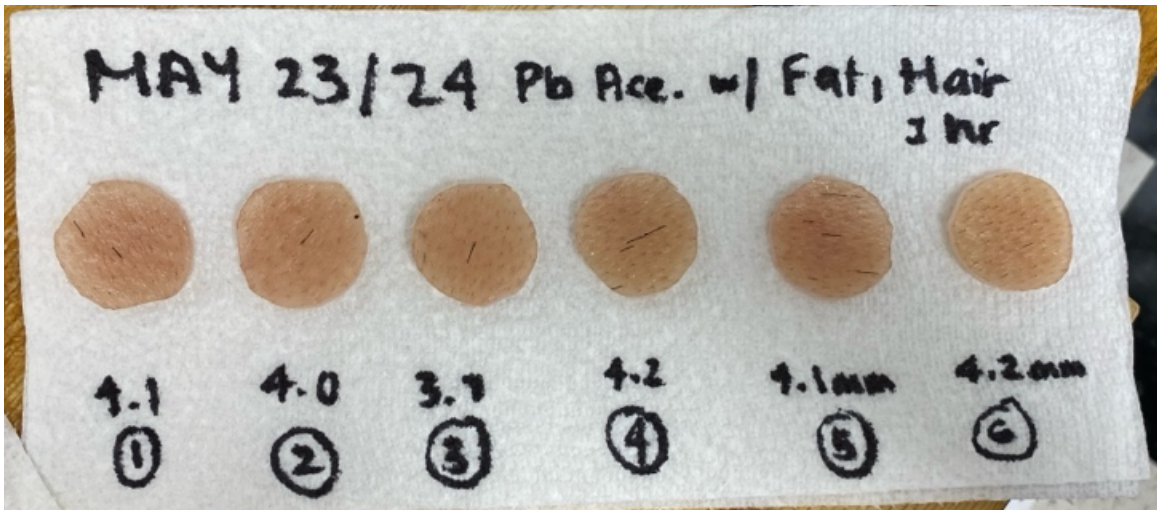

Figure 2.3: Hairy skin prepared for 1 hour of lead diffusion. Samples 1-4 were used to study the effects of a single hair on lead diffusion (with two samples prepared for μXRF measurements), sample 5 was used to study multiple hairs, and sample 6 was used to study the effect of hair follicles without a protruding hair shaft.

2.2.2 Diffusion Experiments

Skin samples were trimmed to a thickness of 2 mm to study the amount of lead passing through the layers of the epidermis and dermis. This follows a typical protocol for transdermal diffusion studies since the outermost layer of the epidermis, the stratum corneum, is considered the rate-limiting barrier to diffusion [19]. Diffusion experiments were performed for skin with hair following the mentioned iterations of hairy skin samples in section 2.2.1, and for skin without hair for comparison of total lead concentration in the receptor solution following diffusion.

Using a micropipette, 100 µL of the 0.33 g/mL lead acetate solution was applied to the skin through the donor compartment of each Franz cell. The donor compartments were sealed, even though experiments were performed in a clean room, to further avoid contamination from any airborne lead particles or dust, and to prevent samples from drying out. The applied lead solution was allowed to diffuse through the epidermis into the dermis and subsequently the receptor solution for either 24, 48, or 72 hours. Time points were selected to be comparable to previously acquired data from our lab for skin without hair, and to extend the data to produce a diffusion curve.

At the end of the diffusion time, the donor compartments where uncovered and any excess lead solution on the epidermis was dried with a sterile cotton bud. The skin from each Franz cell was collected and disposed of as lead contaminated waste. The solution in each receptor chamber was collected into polyethylene vials which were sealed and stored in a fridge (4°C) until they were sent to Kinectrics (Etobicoke, Ontario) for ICP-MS analysis of total lead content at the ppm (µg/g) level.

2.2.3 Synchrotron Experiments

Skin samples were trimmed to a thickness of 4 mm to be able to observe the passage of lead through the skin into the subcutaneous fat layer. This skin thickness was also selected to ensure that the hair follicle was included in the lead pathway, as vellus hairs are said to reach a depth of 1 mm into the dermis and terminal hairs are said to reach a depth of 3 mm or more in the hypodermis [62]. In addition, previous data from our lab has shown specific lead uptake in structures within the subcutaneous fat layer which we aimed to replicate and study. Diffusion experiments were performed for skin with hair following the mentioned iterations of hairy skin samples seen in figure 2.3. Comparisons of the synchrotron x-ray imaging results of hairy skin diffusion to hairless skin diffusion will be made in a future work.

The 0.33 g/mL lead solution was applied to the skin through the donor chamber as in section 2.2.2 and the donor compartments were sealed. The applied lead solution was allowed to diffuse through the epidermis into the dermis and subcutaneous fat layer for either 0.25, 0.5, 1, 2 or 24 hours. These time points were selected to capture the early phases of lead diffusion through skin with hair, as it was found that lead was able to reach the bottom surface of the dermis within 4 hours of diffusion in a previous μXRF data acquisition, as stated in an undergraduate thesis from our lab [63]. In addition, the literature suggests that if the follicle has effects on the diffusion of solutions into the skin, then the effects of the follicle will be saturated within the first 30 minutes of diffusion [64].

At the end of the diffusion time, the donor compartments were uncovered and any excess lead solution on the epidermis was dried with a sterile cotton bud. The skin from each Franz cell was collected onto separate, paper towel-lined petri dishes to avoid cross-contamination between samples. The skin was trimmed to leave only the area of the skin which was aligned with the opening of the donor and receptor chambers and thus involved in the lead diffusion. The skin remaining after trimming was flash frozen using liquid nitrogen and stored in separate sealed polyethylene vials on dry ice until the sample vials were transferred to a -80°C freezer.

Flash-frozen skin samples were prepared for cross-sectional μXRF analysis following a modified protocol for cryosectioning fresh frozen tissue [50, 65]. Skin sectioning was performed at the John Mayberry Histology Facility at McMaster University using the Leica cryostat. The optimal cryosectioning temperature for skin and fat are reportedly different, but a recommended cutting temperature of around -30°C was used [66]. In addition, a cube of dry ice was held against the skin immediately before slicing to ensure all the layers of the skin and fat were cold enough to obtain a smooth cut. Hairy skin was positioned on the chuck for sectioning at 45° to the blade, with the epidermis facing the blade, ensuring that the follicle would pass through the blade ahead of the protruding hair shaft. Skin cross sections were cut to 25 μm and were transferred to the film portion of specialized XRF slides, which were stored at -80°C until they were freeze-dried.

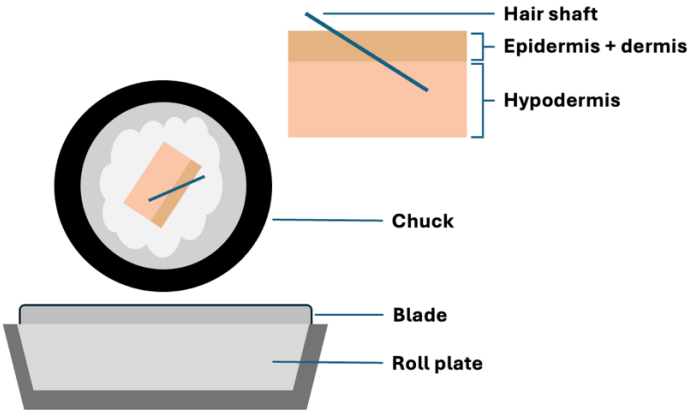

Figure 2.4: Position of a hairy skin sample relative to the blade during cryosectioning.

Specialized XRF slides for sample imaging were prepared in-house. 4 µm thick Ultralene XRF film was affixed to 3D-printed frames using glue. The initial slide frame design followed the dimensions of a conventional microscope slide. Slide frames were later adapted to a ring-like shape to ease sample positioning. Slides in the new format could be rotated in a holder when mounted on the beam line for better alignment.

Figure 2.5: A custom ring-format µXRF slide with hairy skin sections positioned in a custom slide holder for µXRF imaging. The custom ring holder is positioned in the

Thorlabs mounting attachment for the PUMA beamline at Synchrotron Soleil. Ring-format μXRF slides have an inner diameter of 21 mm.

2.3 Free Hair Experiments

Undyed and unbleached cut hair samples of various pigmentation were collected from a hair salon in Vaughan, Ontario. Human ethics approval was not required for collection per the advice of the McMaster Research Ethics Board as no identifying information was obtained for hair donors, and the hair had been marked for waste disposal. The absorption of lead into the hair shaft was studied for one sample of each hair colour: brown, blonde, and grey.

Sections of approximately 50 mm long were excised from the midsection of each collected hair sample using a scalpel to ensure there was no contamination on the cut ends of the hair from the instruments used in the initial hair collection at the salon. The excised sections were split into 4 equal groups, with 2 groups subjected to a cleaning procedure and 2 groups left unwashed. Within the washed and unwashed groups, one of the two groups was treated with a 25% (w/w) lead acetate solution while the other was left untreated. Data discussed in this thesis focuses on the washed samples which were left untreated and washed samples that were treated with a lead solution.

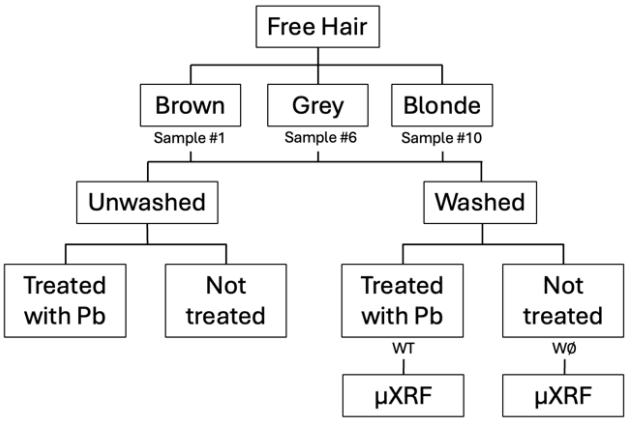

Figure 2.6: Schematic describing the preparation of free human hair samples used for µXRF analysis.

Washed samples were cleaned following a modified version of the procedure outlined by Razagui [67]. Samples were separated into 50 mL centrifuge tubes. 30 mL of isopropyl alcohol was added to each sample tube. Tubes were sealed and placed in an ultrasonicator tub and sonicated at 60ºC using the extensive cleaning setting for 5 minutes. The isopropyl alcohol was then decanted and replaced with 50 mL of deionized water. The sample tubes were resealed and the sonication was repeated. The deionized water was decanted and the process was repeated two more times. After the final sonication in deionized water, each hair sample was collected onto filter paper and rinsed 3 times with 30 mL of isopropyl alcohol. The rinsed hair was then transferred to loosely folded filter paper on a petri dish to airdry overnight. After drying, the untreated samples were transferred to small plastic bags for storage.

2.3.1 Lead-Treated Hair Samples

Using a syringe, 1 mL of the 25% (w/w) lead acetate solution was applied to the center of a fresh petri dish. Holding the hair sample at both cut ends using tweezers, the midsection of each sample intended for lead treatment was dipped into the droplet of lead solution. The hair was rotated in the lead solution for a few seconds to ensure equal application of the lead solution on all surfaces of each hair cuticle in the sample to mimic the application process of lead-containing hair dyes. Care was taken to ensure the solution was not applied to the cut ends of the hair to avoid uptake from exposed ends of the hair shaft. A new petri dish with 1 mL of the lead solution was prepared for each sample to avoid cross-contamination. The dipped hair was transferred to loosely folded filter paper on a petri dish to airdry for 72 hours. Once dry, the hair was collected into small plastic bags for storage.

2.3.2 Hair Cross-Sectioning

Cross sections of the free hairs were prepared following a modified version of the protocol used by Lorentz et al. [68]. Hair embedding and cross-sectioning was performed at the Canadian Centre for Electron Microscopy (CCEM) at McMaster University. Sections of about 10-20 hairs were taken from each sample. Approximately 1 cm of hair was excised from the midsection of each hair sample and positioned into a resin mould according to their respective sample label. Spurr's Resin prepared by Marcia Reid at the CCEM was added to each sample well in the mould, which was then transferred to a vacuum oven for

1 hour to allow the resin to penetrate the cuticle layers. The resin mould tray was then transferred to a 60ºC oven to polymerize for 24 hours.

Once polymerized, the resin embedded hair samples were cross-sectioned to a thickness of 10 µm using an ultramicrotome equipped with a glass blade. Sectioned hair was first transferred to a dish of warm water, then transferred to an XRF slide. The samples were allowed to dry on the slides under a warm lamp for approximately 30 minutes. Slides were stored in regular microscope slide containers.

2.4 Beamline Description

The PUMA ("Photons used for Ancient Materials") beamline at Synchrotron Soleil was used for the collection of data pertaining to the effects of hair on lead absorption through skin [69]. The PUMA beamline uses a 1.8 T wiggler as the radiation source, followed by a 300 µm beryllium window to filter x-rays below 1 keV. After passing through the primary slits, the apertured beam is horizontally focused. The beam energy is selected by a double crystal monochromator where a Si(111) crystal was selected for this experiment to probe the lead L-series. The beam is further apertured by tertiary slits, then the beam is focussed to a focal spot size of 5 µm (vertical) x 7 µm (horizontal) on the sample by a Kirkpatrick-Baez (KB) micro-focussing mirror system designed in-house at Synchrotron Soleil. Downstream, the sample is positioned at a 45º angle to the incoming beam on a motorized stage which can be controlled remotely for precise sample positioning and sample rastering. A microscope perpendicular to the sample allows for remote visualization

of the sample position. A 450 µm thick silicon drift detector (SDD, Rayspec) was positioned at a 90° configuration to the incoming beam to collect the fluorescence signal for both µXRF imaging and XAS. To avoid oversaturation of the detector, the detector was positioned 8 cm away from samples with high lead content, or 3.5 cm away for samples with low lead content. Data acquired for standard reference materials for µXRF imaging and XAS were acquired at a distance of 8 cm from the detector.

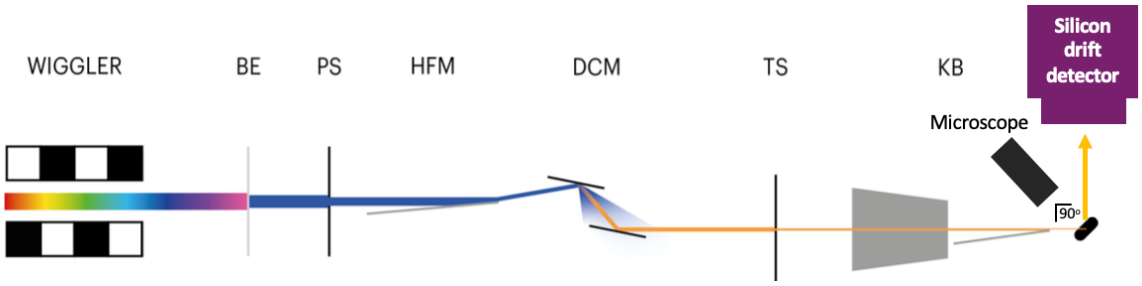

Figure 2.7: Visual representation of the beam path through tuning and focussing components, as well as from the sample to the detector for the PUMA beamline at Synchrotron Soleil. This figure was adapted from Schöder et al. [69].

2.4.1 µXRF Mapping

Once samples were positioned along the beam path, the sample was brought into the focus of the microscope and the region of interest for imaging was selected using coordinate positions of the motorized stage. Regions for hairy skin samples were selected to include the entire hair shaft in the skin slice, as well as the full length of the skin slice from the epidermis to subcutaneous layer. Regions for free hair samples were selected to include as many of the dispersed hair cross sections as possible. Images for each sample

were either acquired at 20 μm step size using a 50 ms dwell time (coarse resolution, 20x20 μm) or 5 μm step size using a 100 ms dwell time (fine resolution, 5x5 μm). The sample-to-detector distance was adjusted to 8 cm for hairy skin samples or 3.5 cm for free hair samples in order to limit the detector deadtime to < 20% while obtaining sufficient lead counts. The NIST 610 standard reference material was imaged using μXRF for comparison with the hairy skin and free hair μXRF data since its lead content is known. For the standard, the detector distance was set to 8 cm, with μXRF imaging data acquired at 20 μm step size using a 100 ms dwell time.

μXRF spectra were analyzed using the shareware PyMCA program and subsequently Matlab. Using PyMCA, the collected spectra were fit using a combination of elements that were likely to be found within the skin and hair, taking into account beam parameters such as composition of elements the beam passed through upstream of the sample and their distances, and estimated sample matrix composition. For quantification, fundamental parameters like flux, dwell time, detector active area, sample matrix and distance to the detector were also included in the spectral fitting procedure [70]. From the spectral fit, elemental maps could be extracted.

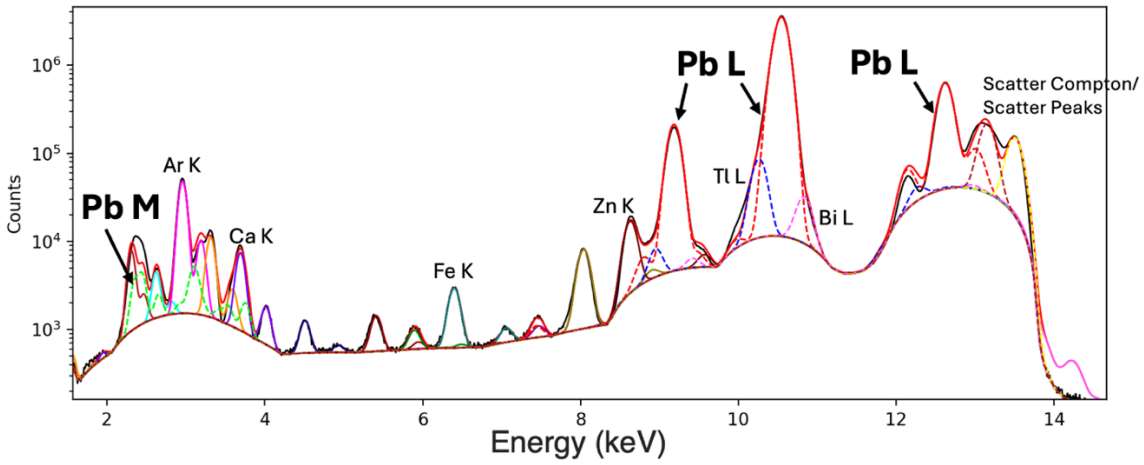

Figure 2.8: XRF spectrum for a hairy skin sample following 1 hour of lead acetate diffusion. The spectrum is shown on the logarithmic scale to be able to visualize elements other than lead.

2.4.2 XAS Measurements

Six powdered lead compounds ($Pb(CH_3COO)_2$, $PbCl_2$, Pb_3O_4, PbO, PbO_2, $PbCO_3$) were used as standard reference compounds for XAS. The powders were weighed and diluted with cellulose to give an absorption edge jump of 1.6 following the standard protocol for XAS standards from the Stanford Synchrotron Radiation Lightsource (SSRL) [71]. The diluted compounds were pressed into thin disks and sealed in clear tape to be measured.

At the PUMA beamline, standard XAS spectra are obtained in fluorescence mode rather than transmission mode due to the configuration of the experimental hutch. The standards were positioned downstream at 45° to the incoming beam as previously described

and their fluorescence was detected with the SDD. In this set-up, a μXRF image was taken of a small section of the standard sample, then a pixel with the least intense signal on the lead map was chosen for measuring the XAS spectra of the standards. The least intense pixel was selected so that there was no self-absorption in the XANES spectrum. All standard XAS measurements were taken once for each standard.

XAS spectra for the skin samples were collected immediately following their corresponding μXRF map acquisition to maintain accurate positioning of the sample with respect to the beam. XAS measurements for skin samples were only taken for specific regions of interest, including high intensity pixels on the lead maps, the front and/or back surfaces of the skin, and specific structures. The spectra were recorded with a 2 second dwell time in 5 eV steps for the pre-edge region (12.95-13.02 keV), and 1.5 eV steps across and beyond the edge (13.02-13.2 keV) to achieve a smooth curve for the L_3-edge.

XAS spectra were analyzed using the Larch program. All spectra were normalized and compared by linear combination fitting (LCF) using the spectra obtained from the lead standards in the fitting model.

3 Results

3.1 General Results

The only visible change to the skin surface following Franz cell diffusion was minor swelling which coincided with the position of the donor cap vestibule on the skin. This was observed for experiments using lead acetate as the donor solution, as well as for control experiments which used deionized water as the donor solution. For hair samples treated with a 25% (w/w) lead acetate solution, there was limited visible colour change to the hair upon application or at any time afterwards.

All ICP-MS analyses were performed by Kinectrics in Etobicoke, Ontario. Non-zero ICP-MS results for analysis of total lead content in the Franz cell receptor solution shows that lead can pass through the layers of hairy skin within 24 hours.

Prepared XRF skin sample slides aimed to include the hair from follicle to the superficial end of the hair shaft, however this was not always possible as the hair often shifted within the skin during cryosectioning, or the underlying hair in the sample was not positioned exactly parallel to the cutting blade. Thus, all μXRF images of hairy skin include a portion of the underlying hair, but not always the entire hair shaft.

All μXRF data was normalized to the ion chamber upstream from the sample to account for any beam intensity variations and corrected for detector dead time using a script provided by Dr. Sebastian Schöder, the PUMA beamline scientist. During acquisition, it was attempted to maintain the detector deadtime below 20% by changing the sample-to-detector distance to 8 cm for hairy skin samples. The goal of keeping deadtimes low was

to ensure that a script using either a paralyzable or non-paralyzable model of deadtime behaviour would accurately correct the signals to account for the detector deadtime. However, high lead content of the skin samples at long diffusion times (24 hours) caused deadtime to rise to a maximum of 44% at an 8 cm sample-to-detector distance, corresponding to the regions of highest lead concentration. Areas of high lead content in the samples as measured by the detector may not always be due to high diffusion into skin, but may also be attributed to the unavoidable folding of the sample onto itself during the XRF slide preparation process.

Calculations for lead concentration from μXRF data were performed using the PyMCA software, and the matrices of the lead concentration for each pixel were exported as comma separated value matrices and analyzed further using Matlab.

3.2 Receptor Solution ICP-MS Results

The receptor solution collected following the diffusion of a 0.33 g/mL lead acetate solution through the epidermis and dermis of hairy skin was analyzed using ICP-MS for total lead content. Matched diffusion experiments using hairless skin were also sent for ICP-MS analysis. Data was reported in ppm (μg/g) with the results listed below.

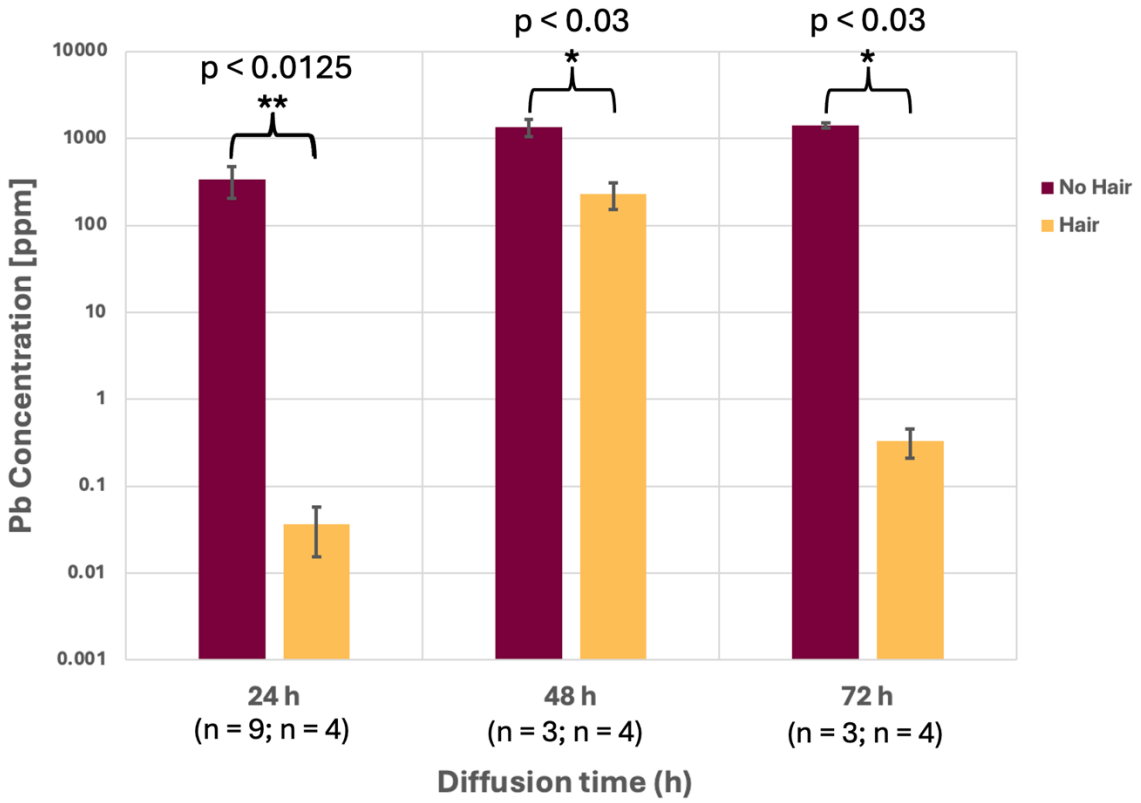

Figure 3.1: Average concentration of lead found in the Franz cell receptor solution following a lead diffusion time of 24, 48, or 72 hours. Data is displayed for both hairy and hairless skin. Error bars represent the standard error of the mean.

Figure 3.1 displays the average concentration of lead for each sample type at each time point, with the error bars representing the standard error of the mean. Although there is evidence that the data are non-normally distributed, mostly due to small sample sizes, the average and median values were very similar in most cases.

Since a linear region does not exist for this diffusion data for skin with hair, a K_p could not be calculated. Skin samples without hair were observed to consistently show greater concentrations of lead in the receptor solution following the listed diffusion time

periods compared to hairy skin. Results of the Mann Whitney U Test determined that the differences in the mean lead concentration between hairy and hairless skin were statistically significant at the 97% confidence level for lead diffusion times of 48 and 72 hours, with statistically significant differences at the 98.75% confidence level for the 24-hour lead diffusion samples.

3.3 Synchrotron Results

3.3.1 Standards

A μXRF image was acquired for the U.S. National Institute of Standards and Technology (NIST) 610 standard reference material, whose composition is well-documented with respect to the mass fractions of various elements contained in the standard, including lead [72]. Using PyMCA, the XRF spectrum averaged by the number of pixels in the μXRF image was used to create a spectral fitting configuration file to estimate the beam flux reaching the sample. The configuration file considers the beam energy (13.5 keV), the expected elements for characteristic x-ray emission as listed on the NIST 610 data sheet, materials in the beam path that may attenuate the beam as it travels to the detector, as well as the fundamental parameters such as the distance travelled along the beam path (8.075 cm), the detector active area (80 mm^2), and the dwell time (100 ms). The glass matrix of the standard reference material (72% SiO_2, 14% Na_2O, 12% CaO, 2% Al_2O_3) was also included in the fitting configuration. The flux parameter was iteratively adjusted to match the elemental mass fraction of lead in the standard. The flux is derived

from the measured fluorescence intensity of the standard and its mass fraction serves as a calibration factor to extrapolate the concentration of elements in different samples measured under identical conditions. The flux that was found to produce the standard reference material's known lead mass fraction for the average XRF spectrum was approximately 3.73 x 10^8 photons/s. Flux defined within the PyMCA program is not the absolute flux of the beamline, but instead serves as a scaling factor determined based on the known mass fraction of the element of interest in the standard, measured emitted fluorescence of that known mass fraction, and tabulated atomic constants.

Reference XANES spectra were acquired for linear combination fitting (LCF) analysis following data acquisition. The spectra were normalized and the edge energy (E0) was aligned to the most intense maxima of the first derivative of the normalized μ(E). The normalized reference XANES spectra and their first derivatives are shown below.

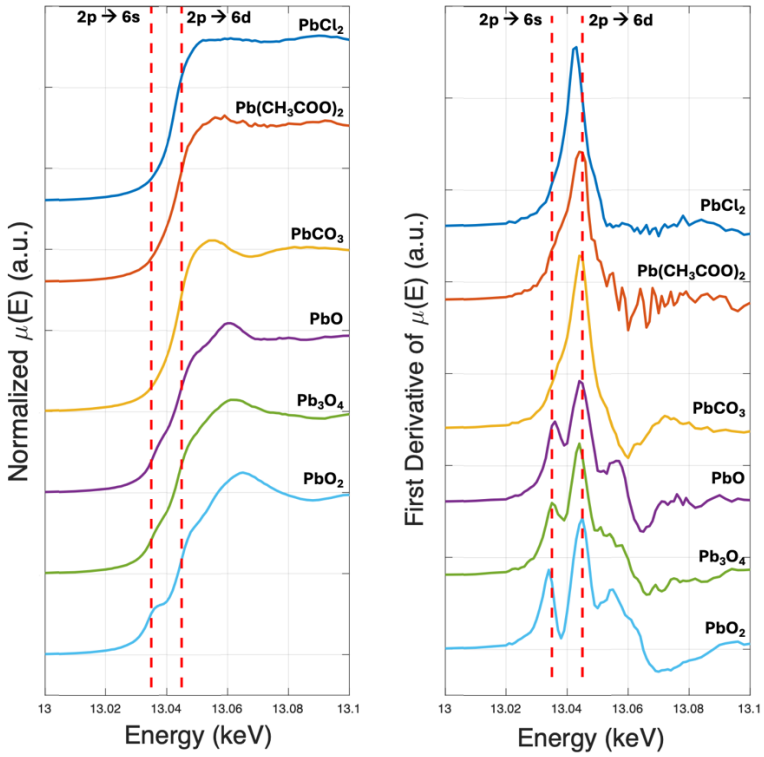

Figure 3.2: Reference spectra for LCF to XANES measurements of the hairy skin samples. The first dotted line (13.035 keV) corresponds to the 2p → 6s transition for tetravalent lead compounds, and the second dotted line (~13.045 keV) corresponds to the 2p → 6d transition for both divalent and tetravalent lead compounds [55, 73, 74].

3.3.2 Skin µXRF

Although skin diffusion experiments were performed for six samples at a time, only 1-2 samples from each experiment were prepared for µXRF imaging. The remaining skin samples from each experiment were analyzed for total lead content using ICP-MS for verification of quantitative analysis performed on the µXRF data using PyMCA.

Spectral fitting was performed on the XRF spectrum averaged by the number of pixels in the μXRF image using PyMCA. A configuration file was created for skin imaging, which considered the beam energy (13.5 keV), elements expected to be incorporated in the skin, and materials in the beam path that may attenuate the beam. An attenuator matrix for skin was created using the elemental components of the skin listed by the International Commission on Radiological Protection (ICRP), as well as the ICRP documented density for the skin (1.1 g/cm^3) [75]. Additionally, the fundamental parameters of distance travelled along beam path (8.075 cm), detector active area (80 mm^2) and dwell time (50 ms for coarse resolution images; 100 ms for fine resolution images) were applied, along with the beam flux of 3.73 x 10^8 photons/s extrapolated from the NIST 610 standard. Elemental mass fraction distribution maps were calculated for each sample by a fast-XRF-fitting function in PyMCA.

Coarse (20x20 μm) scans were acquired for each sample to get an initial idea of the distribution of lead through the sample, with subsequent imaging at finer resolution in areas of interest. Elemental concentration maps computed by PyMCA were plotted using Matlab. These maps display the mass fraction of the element of interest, which is reported for each image pixel in ppm (μg/g).

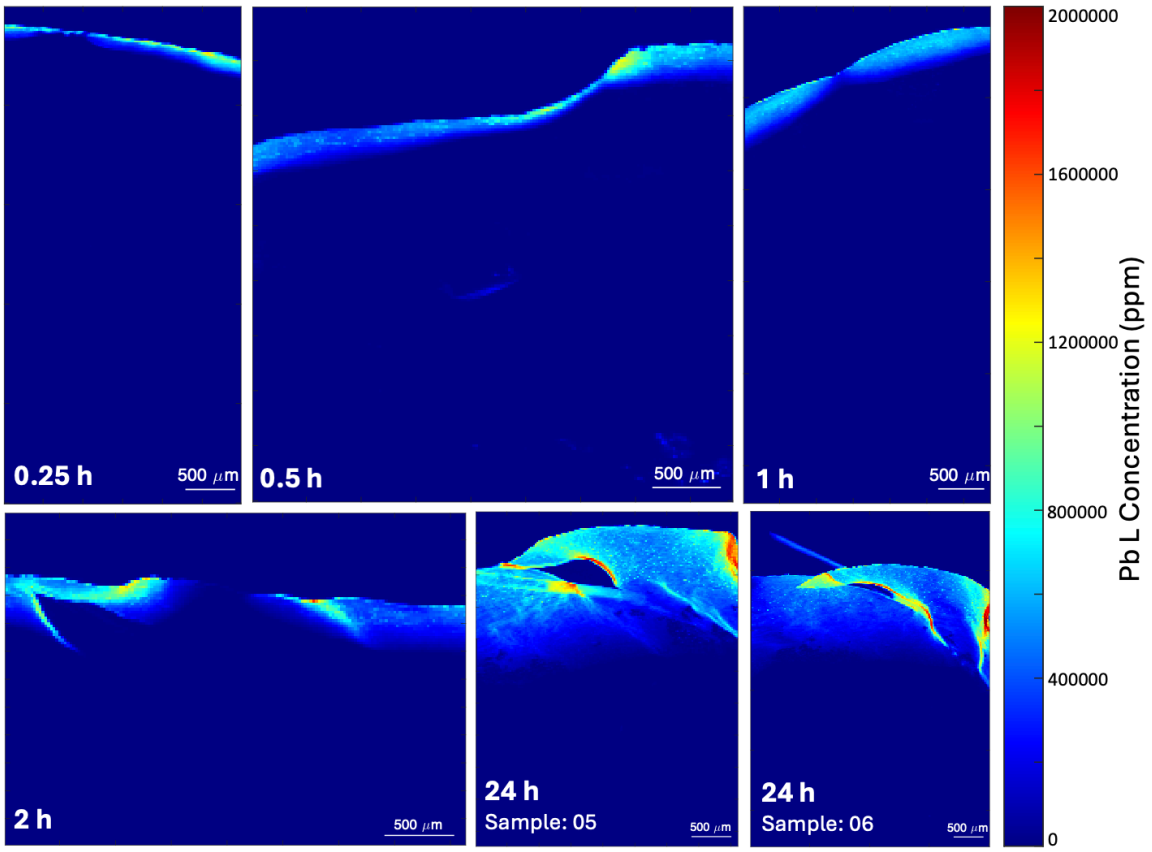

Figure 3.3: Coarse resolution (20x20 µm) maps of the elemental distribution of lead in skin samples subjected to lead acetate diffusion for 0.25, 0.5, 1, 2, or 24 hours. µXRF imaging data was acquired at the PUMA beamline using a 13.5 keV beam energy with 20 µm step size and 50 ms dwell time. Lead distribution maps were produced using a flux of 3.73 x 10^8 photons/s in PyMCA. Two coarse scans were acquired for the 24-hour diffusion time from adjacent cross-sections of the same skin sample.

Lead concentrations calculated for the coarse scans reach intensities as high at 1900000 ppm for the 24-hour diffusion time as calculated in PyMCA. Average lead concentrations for each diffusion time were calculated after the removal of pixels in the µXRF image that

were outside of the skin using a masking technique on Matlab. Folds in the sample were not excluded from the data, likely causing the average concentrations calculated in PyMCA to be higher than the true value, as each folded region represents three layers of skin, thus the measured lead concentrations in these regions are a factor of three times greater than the actual concentration. Average lead concentrations for each time point were 16128 ppm, 36774 ppm, 36335 ppm, 50320 ppm, 212124 ppm, and 166829 ppm for 0.25-, 0.5-, 1-, 2-, and 24-hour (sample 5 and 6) diffusion times, respectively. Lead concentration is maximal near the skin surface and in areas where the sample folded over itself during XRF slide preparation. Lead accumulation is also seen in small clusters near the skin surface, most easily seen in the 0.5- and 24-hour samples. Looking at both μXRF and ICP-MS data, it can be seen that lead acetate penetrates into the skin almost immediately, as there is evidence of diffusion to a depth on the order of 100 μm into the skin after 15 minutes of lead application. This depth is greater than that of the stratum corneum, suggesting that this layer of the epidermis is not the primary barrier for transdermal absorption of lead acetate in hairy skin. As diffusion time increases, the lead penetrates deeper into the skin, reaching a maximum depth of approximately 300 μm in 30 minutes, 400 μm in 1 hour, 440 μm in 2 hours, and 1640 μm in 24 hours. As lead penetrates further, more lead diffuses from the applied lead acetate solution into the skin and the total amount of lead in the skin sample increases, with the mass of lead in the skin increasing by a factor of approximately 3 between 15 minutes and 2 hours of diffusion, and a factor of over 10 between 15 minutes and 24 hours.

Additional μXRF imaging beyond the coarse (20x20 μm resolution) maps was performed to investigate the lead diffusion and accumulation of the 0.5-, 1-, 2-, and 24-hour samples using a higher resolution. Fine (5x5 μm) resolution scans were usually acquired at the level of the epidermis and dermis, including the hair follicle underlying the skin surface. Transmitted light microscopy images for each sample were acquired at the Center for Advanced Light Microscopy (CALM) at McMaster University, and are shown with the μXRF maps to verify the presence of the hair follicle beneath the skin surface.

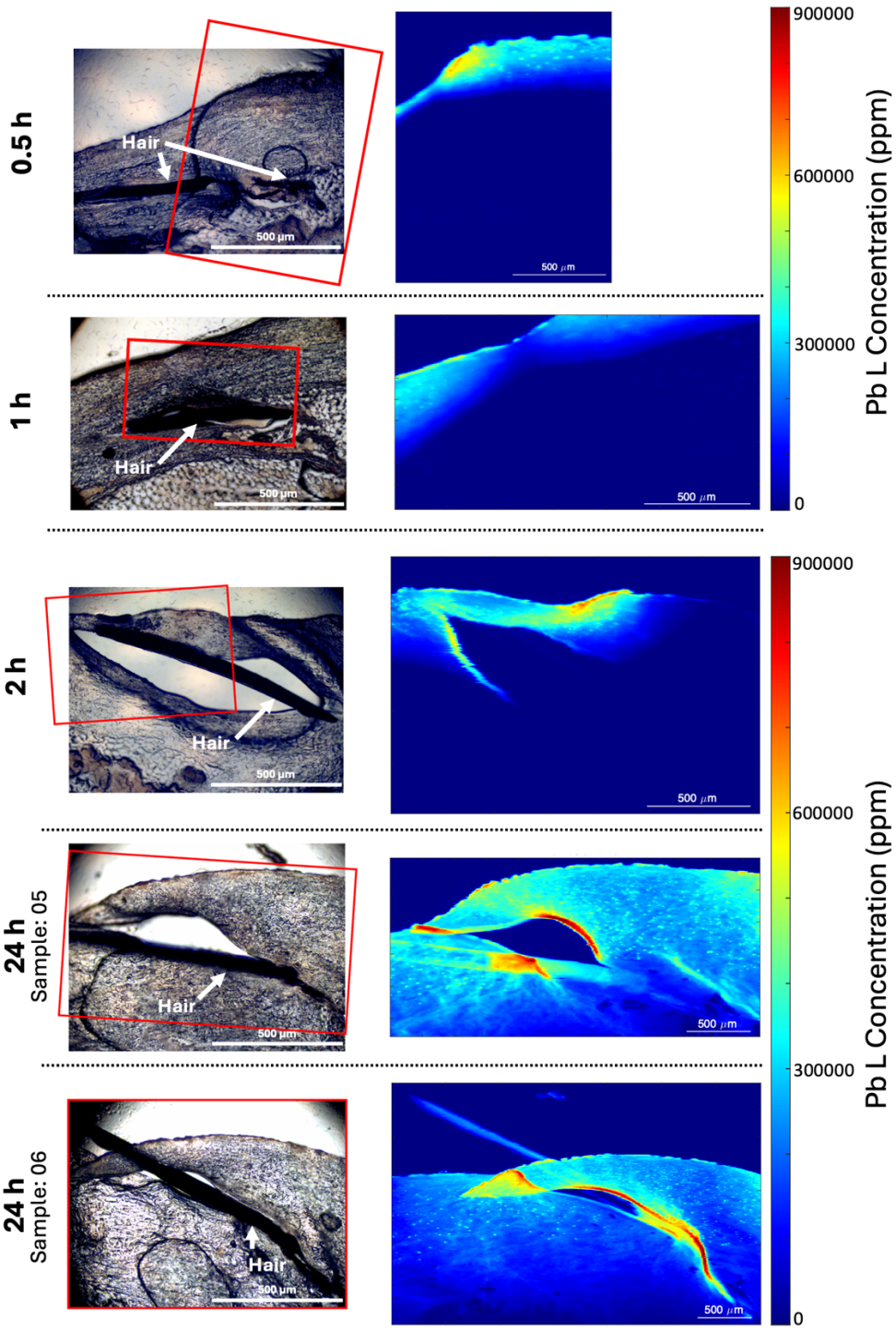

Figure 3.4: Fine resolution (5x5 µm) maps of the elemental distribution of lead in skin samples subjected to lead acetate diffusion for 0.5, 1, 2, or 24 hours. µXRF imaging data

was acquired at the PUMA beamline using a 13.5 keV beam energy with 5 μm step size and 100 ms dwell time. Lead distribution maps were produced using a flux of 3.73 x 10^8 photons/s in PyMCA. All fine scans displayed were acquired for the corresponding sample imaged under coarse scan conditions from figure 3.3. A fine scan was not acquired for the 0.25-hour diffusion time. Transmitted light microscopy was used to verify the presence of subcutaneous structures in the sample, as well as the relative location of the hair below the skin surface.

As with the coarse scans, high concentrations of lead are found at the skin surface where the lead solution was applied, as well as in areas where the sample folded over itself. The accumulation of lead in small clusters in the epidermal and dermal layers of the skin are better resolved in the fine scans. The data were again filtered to remove pixels which were not within the skin to calculate the average lead concentration in the skin. Folds in the sample were not excluded from the data. Average lead concentrations calculated from the filtered data were 41718 ppm, 35214 ppm, 40978 ppm, 122419 ppm and 181081 ppm for 0.5-, 1-, 2-, and 24-hour (sample 5 and 6) diffusion times, respectively. As these are finer scans of the same data, the same pattern of lead diffusing further into the skin over time seen in the coarse scans is observed here.

Hairy skin samples which were not exposed to lead or subjected to the Franz diffusion cell conditions (control samples) were also imaged using synchrotron μXRF under coarse scan conditions. The spectral fitting parameters used for the previous samples were applied in the PyMCA spectral fitting configuration for these control samples, except

the dwell time was adjusted to suit the coarse scan conditions (50 ms). The sample-to-detector distance was decreased to 3.5 cm to detect adequate signal from the sample.

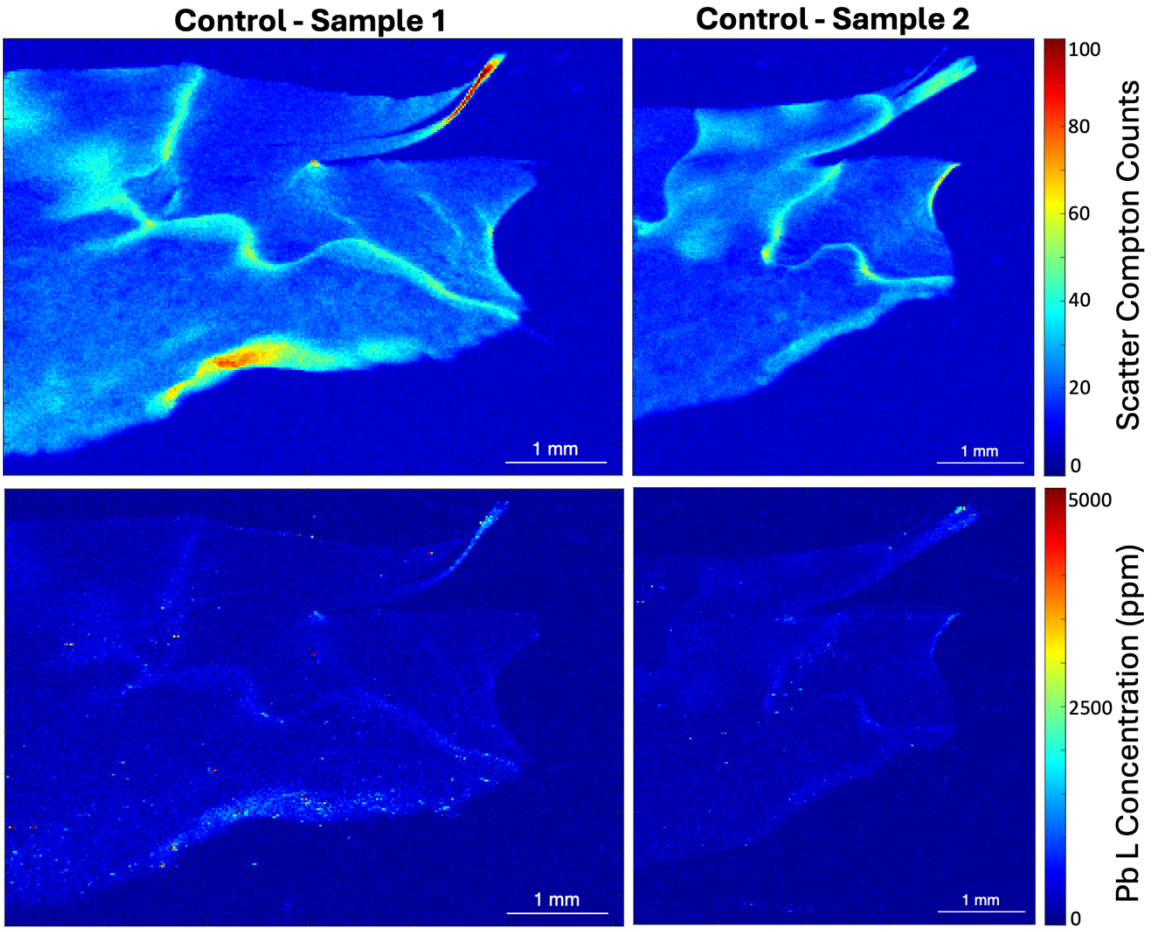

Figure 3.5: Coarse (20x20 µm) µXRF scans of hairy skin samples which were not exposed to lead, nor the Franz diffusion cell set up. Scatter Compton maps (top row) display the detector counts corresponding to the Compton peaks in the µXRF spectrum as calculated by PyMCA using a flux of 3.73 x 10^8 photons/s. As the Compton scatter intensity is proportional to the mass of the sample, these maps are shown to verify the presence of the sample within the imaging area. The lead scale on the lead maps (bottom row) has been

adjusted by over two orders of magnitude compared to the lead-exposed samples to permit the lead signals to be seen in the control sample maps.

Hairy skin samples which were not exposed to lead or Franz diffusion cells produce extremely low lead signals, with an average μXRF-derived lead concentration of 330 ppm and 236 ppm for samples 1 and 2, respectively. For comparison, the average lead levels in human blood, tibia and calcaneus in urban Canadians are approximately 10 ppb, 4 ppm, and 10 ppm, while urban background house dust levels in Canada have median lead levels of 58 ppm and buildings constructed prior to 1980 have shown average dust lead content of around 450 ppm [61, 76, 77]. Maximum lead concentrations as high as 34000 ppm were detected from the μXRF data, which correspond to areas where the sample has folded on itself and thus the signal was multiplied, or where the hair was not flat on the XRF slide and so the lead intensity was increased as the distance to the detector was reduced.

Histogram probability distributions are displayed below for the lead concentration for each pixel in the coarse scans from figure 3.3. Histograms were constructed using data excluding pixels which were not in the skin, and histogram bin widths were restricted to 2500 ppm.

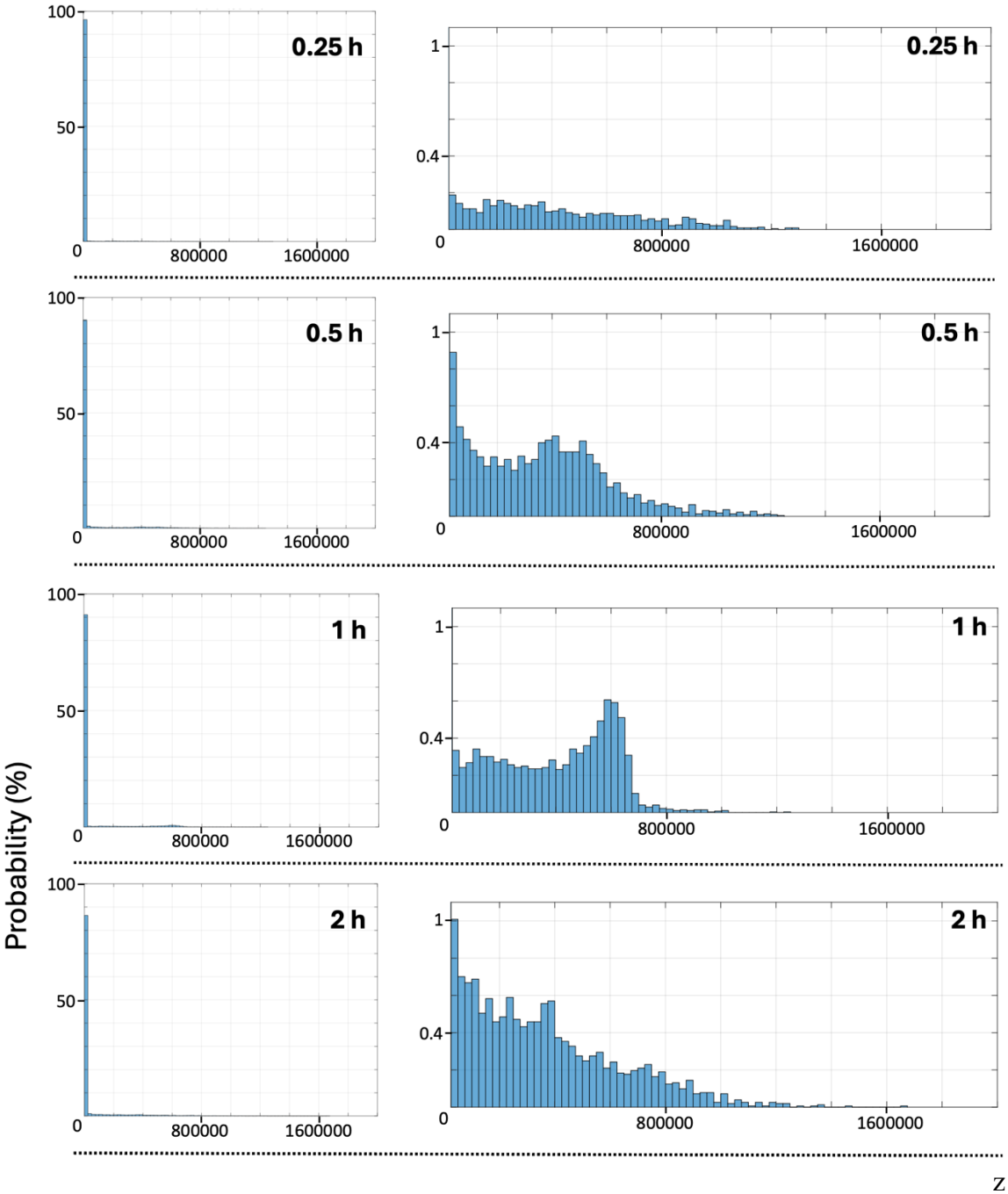
0.25 h
0.25 h
0.5 h
0.5 h
1 h
1 h
2 h
2 h
Probability (%)
z
100
50
0
1
0.4
800000
1600000

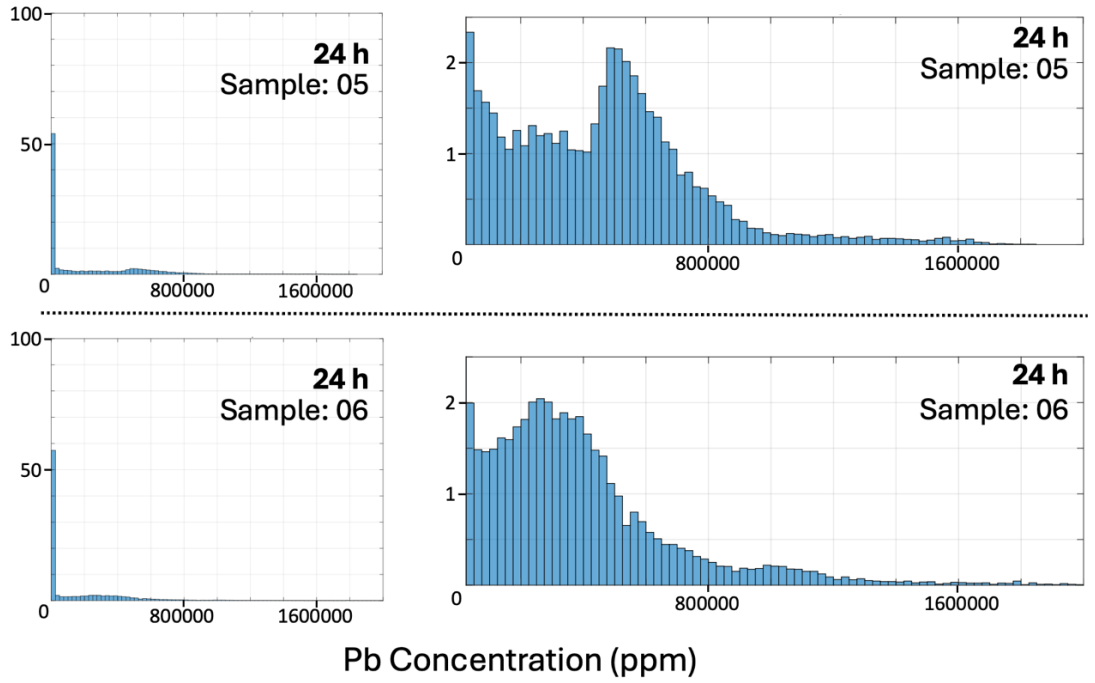

Figure 3.6: Histogram probability distributions of the lead concentration for each pixel in the coarse scans of hairy skin samples from figure 3.3. The plots on the left show the entire distribution, and the plots on the right show the distribution excluding the first histogram bin.

All histograms have a large number of pixels corresponding to the lead concentrations between 0-2500 ppm. This is because the lead is diffusing into the skin from the surface, and the skin towards the back of the sample is at the lead level of the control samples. At short diffusion times, this can be most of the sample. Beyond this range of lead concentration, the distributions for each time point often show at least one distinct peak with the 1-, 2- and 24-hour (sample 5) diffusion times showing a distinct peak occurring between 400000-600000 ppm.

At short time points, it can be seen that the lead diffusion appears to vary depending on the position along the skin surface in relation to the hair underlying the skin surface. For the 1-hour diffusion case, concentration profiles perpendicular to the tangent of the skin surface at various points across the skin surface were plotted as a function of distance from the skin surface towards the dermis. The centroid of the underlying hair was found from the zinc elemental map, and the concentration profile perpendicular to the skin surface which aligned with the position of the centroid was used for statistical comparisons.

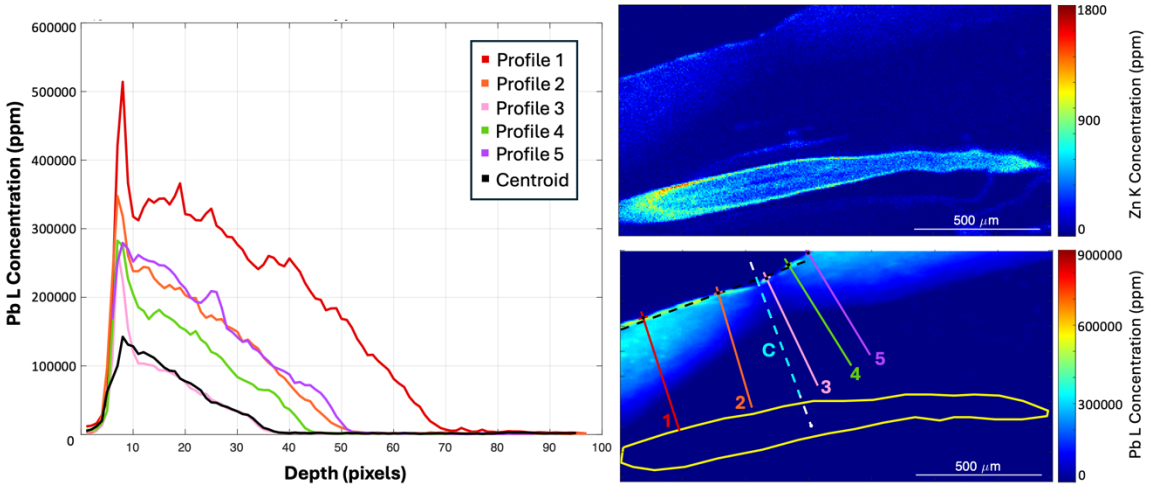

Figure 3.7: Lead concentration intensity profiles from the skin surface towards the subcutaneous layers for a hairy skin sample corresponding to the 1-hour lead diffusion time. An elemental concentration map for zinc (top right) is included to visualize the exact position of the hair beneath the skin for the corresponding elemental concentration map for lead (bottom right). Lead concentration intensity profiles at various positions along the skin surface are illustrated and numbered on the lead concentration map (bottom right), with a dotted line representing the intensity profile from the skin surface towards the centroid of

the underlying hair. The lead concentration intensity profiles are displayed in the plot on the left.

The Wilcoxin Signed-Rank test was applied to the concentration intensity profiles for the 1-hour fine scan μXRF data and was compared to the concentration intensity profile along a line perpendicular to the skin surface corresponding to the position of the centroid of the hair below the skin surface. Significant differences in the lead concentration profiles and thus depth of lead penetration visualized by μXRF were found across the skin surface with respect to the position of the underlying hair in the skin. The presence of the hair appears to alter diffusion.

Table 3.1: Results of Wilcoxin Signed-Rank test for 1-hour lead diffusion concentration profiles from different skin surface locations relative to the hair centroid.

Test Profiles	Critical Value	Test statistic	p-value
Profile 1 vs Centroid	434	5	<0.0001
Profile 2 vs Centroid	434	6	<0.0001
Profile 3 vs Centroid	434	378	<0.0001
Profile 4 vs Centroid	434	46	<0.0001
Profile 5 vs Centroid	434	0	<0.0001

As an additional method for quantification of lead in the skin, ICP-MS analysis was performed on the skin samples remaining after XRF sample preparation. These samples had a diameter of approximately 9 mm and the thickness of about 3 mm. The samples were acid-digested, and thus the results for each sample represent an average value for the lead content throughout the skin rather than a spatially dependent concentration as seen with the μXRF maps.

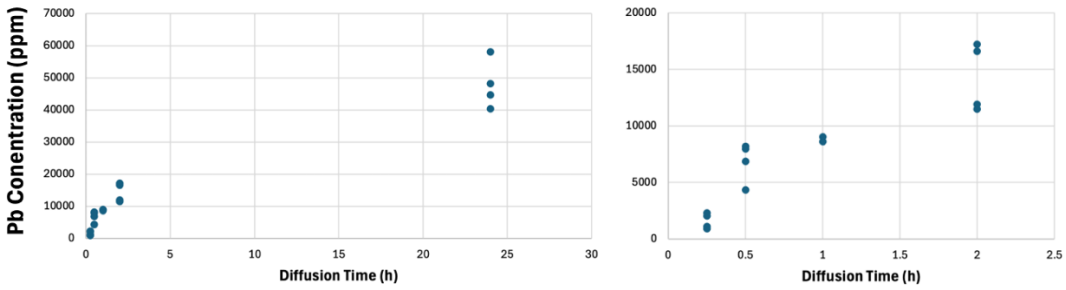

Figure 3.8: ICP-MS results for total lead content in the skin matrix following diffusion times of 0.25-, 0.5-, 1-, 2-, and 24-hours through hairy skin. Both graphs show the same data, but the graph on the right has the x-axis enlarged to show the concentration data for diffusion times less than or equal to 2 hours more clearly.

As expected, the results of ICP-MS analysis of the skin showed increased lead content with increasing diffusion time. Overall, lead concentrations for each time point were on the order of 10^{-3}-10^{-2} ppm. Sample 6 from each experiment yielded the highest lead concentration in all time points except for 0.25 hours. Control samples which were not subjected to Franz cell diffusion or lead yielded lead concentrations below the detection limit of 40 ppm for lead in skin for total sample masses of approximately 0.13 g, as expected.

To understand μXRF-based quantification of lead in the skin samples, the average lead concentrations found from the coarse resolution μXRF maps calculated using a beam flux of 3.73 x 10^8 photons/s were compared to the skin ICP-MS results. Coarse (20x20 μm) images of the skin were used since they are more representative of the entire skin sample from epidermis to subcutaneous layer, and they provide mass fraction outputs from PyMCA on the same order of magnitude as for the fine scans. Moreover, a fine scan was not acquired for the 0.25-hour diffusion sample, thus coarse scans were used for consistency across all

time points. The average µXRF-derived concentrations were compared to the ICP-MS results using a linear regression. A perfect match between the µXRF and ICP-MS results should result in a slope of 1.

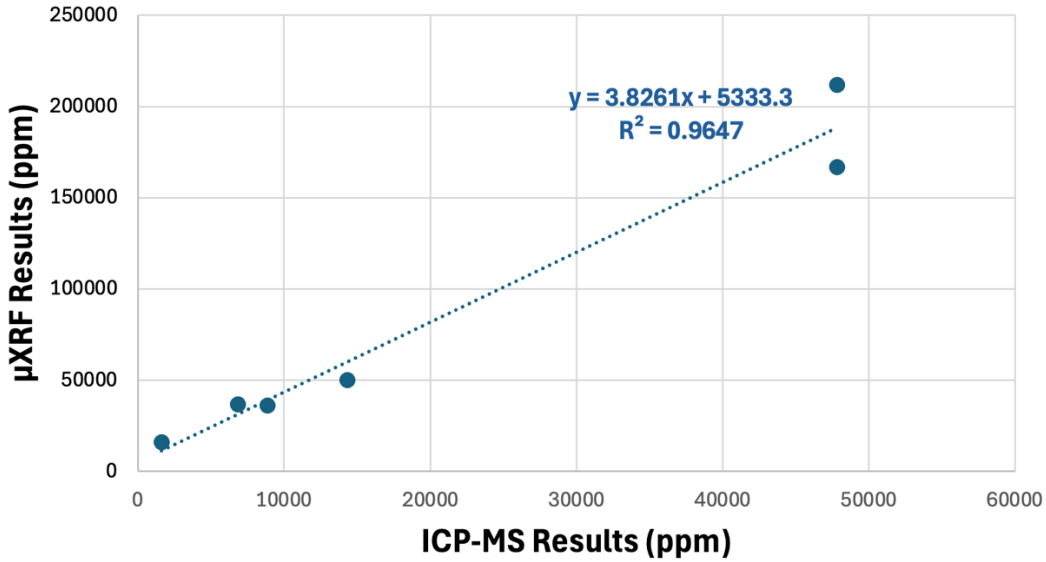

Figure 3.9: The linear regression of the average lead concentration in samples calculated from µXRF maps versus ICP-MS estimates for samples with diffusion times from 0.25 to 24 hours.

Results of the linear regression in figure 3.9 show that the µXRF-derived lead concentrations in the samples are highly correlated with those from ICP-MS ($R^2 = 0.9647$, $p = 0.0005$), however, the slope is approximately a factor of 4 different from 1.

3.3.3 Skin XAS

An investigation of the form of lead in various regions of the skin was performed using XANES measurements. Measurements were taken following the fine μXRF scans of two samples corresponding to a diffusion time of 24 hours as those samples showed the most intense lead uptake and deepest diffusion. XANES measurements were acquired within the hair shaft, along the pore of the hair shaft, and in areas of unusually high lead accumulation. The presented data includes the best fits from a linear combination fitting (LCF) model which utilized the normalized XANES spectra of six reference lead compounds (figure 3.2), computed using the program Larch. The best fit was determined as being the LCF resulting in the lowest χ^2 value, as well as assumptions regarding the likely and possible forms of lead within the skin and skin structures.

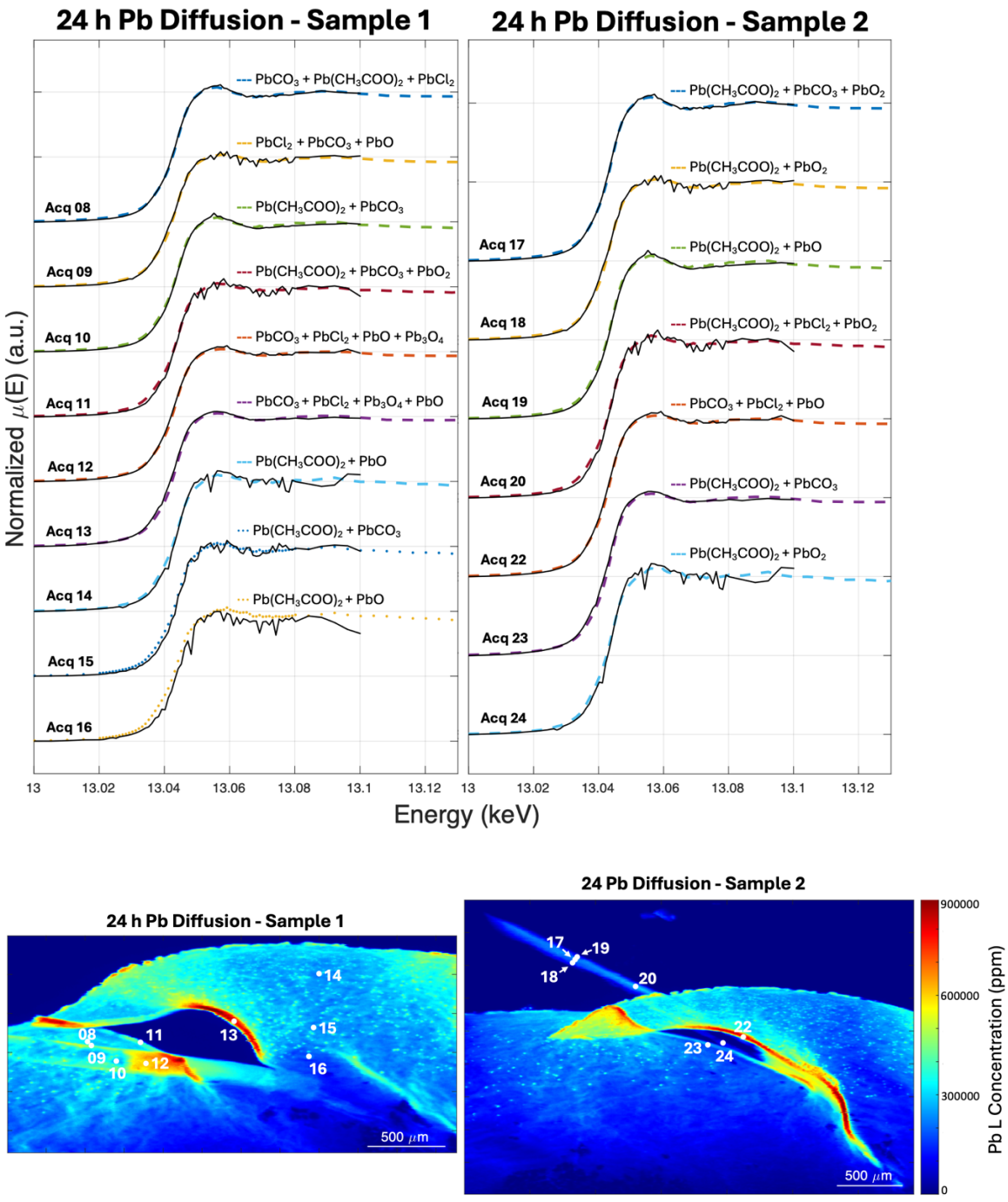

Figure 3.10: Acquired XANES spectra with their LCF results for the corresponding regions on the lead concentration μXRF maps. LCF results for each acquisition are labelled by the reference compounds contributing to the best LCF in order of decreasing weight (left to

right). Positions of the XANES measurements on the samples are labelled in the corresponding lead concentration μXRF maps.

From the LCF results, $Pb(CH_3COO)_2$ is present as the principal component in most regions of the skin, with $PbCO_3$ also reported as a large contributor to the LCF. The lead is predominantly diffusing through skin in the chemical form in which it was applied. Despite the application of lead (II) acetate during Franz cell diffusion, tetravalent lead compounds are common components in the LCF results, including PbO, PbO_2 and Pb_3O_4.

In the LCF process, the fitting model attempts to ensure that the reference spectra weights sum to 1. The weights of each reference spectrum contributing to the best LCF for each acquisition are listed in table 3.2 as percentages.

Table 3.2: Component weights for the LCF of each acquired XANES measurement for 24-hour lead diffusion samples.

24 h diffusion Sample 1									
					% Weight				
Compound	**8**	**9**	**10**	**11**	**12**	**13**	**14**	**15**	**16**
$PbCl_2$	16.45	37.18	-	-	39.16	37.87	-	-	-
$Pb(CH_3COO)_2$	24.82	-	56.31	61.11	-	-	100	79.99	79.39
$PbCO_3$	58.73	35.44	43.69	31.41	39.17	48.90	-	20.01	-
PbO	-	27.38	-	-	15.01	6.00	3.60	-	20.61
Pb_3O_4	-	-	-	-	6.66	7.22	-	-	-
PbO_2	-	-	-	7.48	-	-	-	-	-
24 h diffusion Sample 2									
					% Weight				
Compound	**17**	**18**	**19**	**20**	**22**	**23**	**24**		
$PbCl_2$	-	-	-	11.73	35.90	-	-		
$Pb(CH_3COO)_2$	74.87	86.01	100	78.04	-	73.44	85.74		
$PbCO_3$	14.73	-	-	-	45.42	26.56	-		
PbO	-	-	4.89	-	18.69	-	-		
Pb_3O_4	-	-	-	-	-	-	-		
PbO_2	10.40	13.99	-	10.23	-	-	14.26		

Overall, lead acetate contributes to the LCF in twelve of the sixteen acquired XANES measurements. In all but one of these LCF, lead acetate is found to be the greatest contributor to the LCF, contributing over 50% of the signal in most fits. In sample 1, $PbCl_2$ is only present in the LCF when $PbCO_3$ is also included. $PbCO_3$ is also present in many LCF, and in many cases is the highest contributing component to the LCF, except in those samples where lead acetate is present. PbO often appears in the LCF for the XANES measurements in sample 1, while PbO_2 is the most common tetravalent lead compound contributing to the LCF in sample 2. Pb_3O_4 only appears in the LCF for XANES acquired from sample 1. Overall, tetravalent lead compounds are rarely found to contribute more than 20% to the LCF. The LCF compound weight results add up to 100% in most samples except for acquisitions 13, 14, 19 and 22. In XANES from the ovular lead accumulation sites (acquisitions 14-16), lead acetate contributes to 79-100% of the best LCF, accompanied by either $PbCO_3$ or PbO. In XANES measurements corresponding to the hair in sample 2 (acquisitions 17-19 and 24), lead acetate dominates the LCF, often along with a small (>15%) contribution to the fit from PbO or PbO_2.

3.3.4 Hair μXRF

The average XRF spectrum for each free hair sample was analyzed by spectral fitting in a similar manner to the spectral fitting for the skin samples. Differences in the hair configuration file include the list of elements expected to contribute to the XRF spectrum, the distance travelled along the beam path (3.575 cm), and a new attenuator matrix was created for the hair. The hair sample matrix was created using the reported average

elemental composition of the hair matrix, which includes 45% C, 28% O, 15% N, and 5% S, and the reported dry hair density of 1.32 g/cm^3 [78, 79]. The beam flux determined using the NIST standard (3.73 x 10^8 photons/s) was used in the initial analysis of the hair μXRF data, followed by a comparison to the ICP-MS data for cut hair samples to test the correlation of the results. Elemental mass fraction distribution maps were again produced by the fast-XRF-fitting function in PyMCA. The lead and sulfur elemental concentration maps resulting from further data manipulation in Matlab are shown below in units of ppm (μg/g).

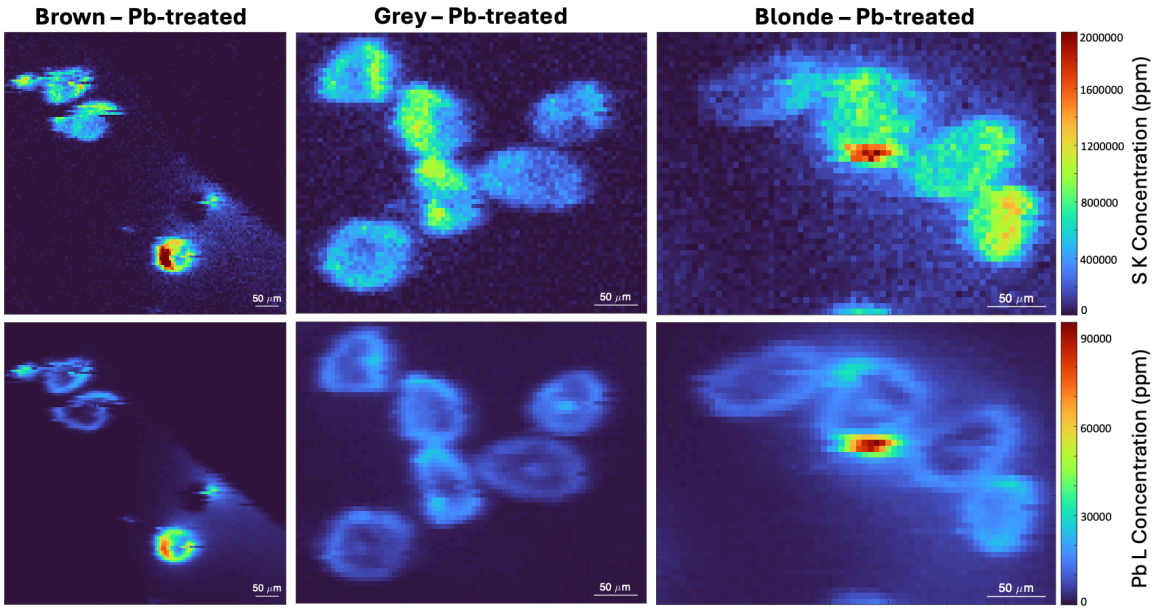

Figure 3.11: μXRF elemental concentration maps for human hair samples that were subjected to a cleaning procedure, then treated with a lead solution. Elemental concentration distributions are shown for sulfur (top row) and lead (bottom row) for brown (left), grey (middle), and blonde (right) hair cross sections. μXRF imaging data was acquired at the PUMA beamline using a 13.5 keV beam energy with 5 μm step size and

100 ms dwell time. Concentration maps were produced from a PyMCA analysis using a beam flux of 3.73 x 10^8 photons/s. Sulfur maps are shown to indicate the location of the hair cross sections in the image.

In figure 3.11, lead is seen to accumulate along the cuticle as well as in the medulla for all hair samples. The lead does not accumulate to a high degree in the cortex. Average lead concentrations in the hair samples were calculated after removing pixels outside of the hair cross sections. Using a beam flux of 3.73 x 10^8 photons/s, the flux derived from the analysis of the NIST 610 standard reference material, the resulting average lead concentrations were 14818 ppm for brown hair, 9606 ppm for grey hair, and 12018 ppm for blonde hair. Although the characteristic energies of the lead M edge emission fluorescence lines are near that of the sulfur K edge, the maximum level of sulfur content computed by PyMCA is comparable to the literature value for sulfur content in the hair matrix (5%) [78].

Control hair samples were also imaged using μXRF to ensure that exogenous lead was adequately removed from the cuticle during the washing process, and to ensure that endogenous lead in the hair matrix was not attributed to the lead solution treatment. Control samples in figure 3.12 were also produced using the beam flux found from the NIST standard (3.73 x 10^8 photons/s), and show extremely low levels of lead in the hair matrix, as expected.

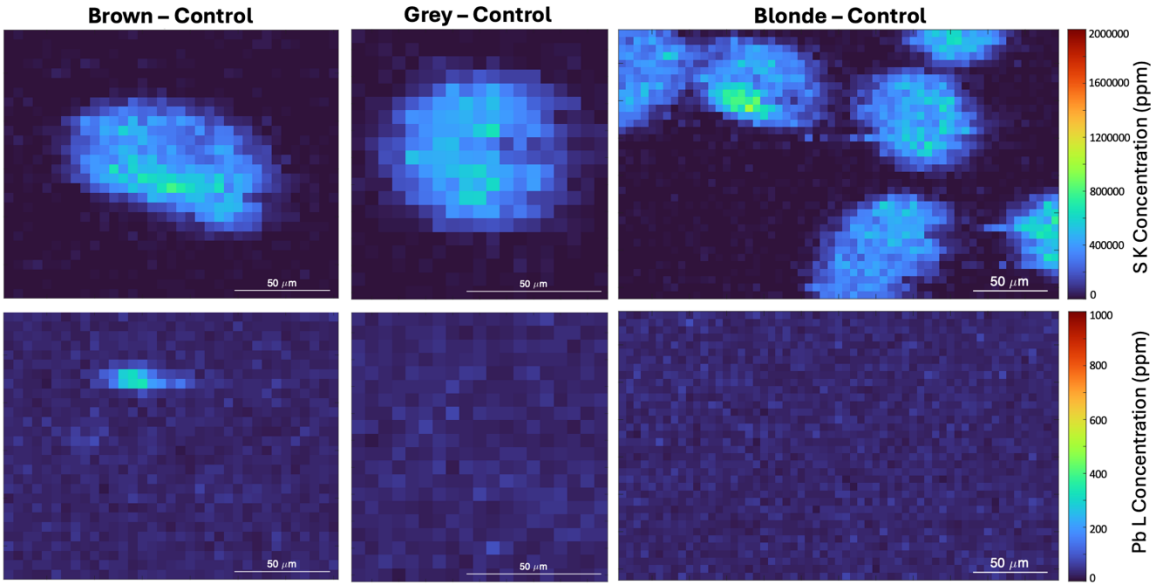

Figure 3.12: μXRF elemental concentration maps for human hair samples that were subjected to a cleaning procedure. Elemental concentration distributions are shown for sulfur (top row) and lead (bottom row) for brown (left), grey (middle), and blonde (right) hair cross sections. μXRF imaging data was acquired at the PUMA beamline using a 13.5 keV beam energy with 5 μm step size and 100 ms dwell time. Concentration maps were produced from a PyMCA analysis using a beam flux of 3.73 x 10^8 photons/s. These samples were prepared from the same hair samples as the brown, grey and blonde lead-treated samples prior to lead treatment.

Average lead concentrations in the untreated hair samples were calculated after removing pixels outside of the hair cross sections. Using a beam flux of 3.73 x 10^8 photons/s, the resulting average lead concentrations were approximately 39 ppm for brown hair, 32 ppm for grey hair, and 32 ppm for blonde hair.

Histogram probability distributions are displayed below for the lead concentration per pixel in the fine scans of lead-treated human hair samples. Histograms were constructed using data which excluded pixels that were not in the hair cross sections. Histogram bin widths were restricted to 2500 ppm.

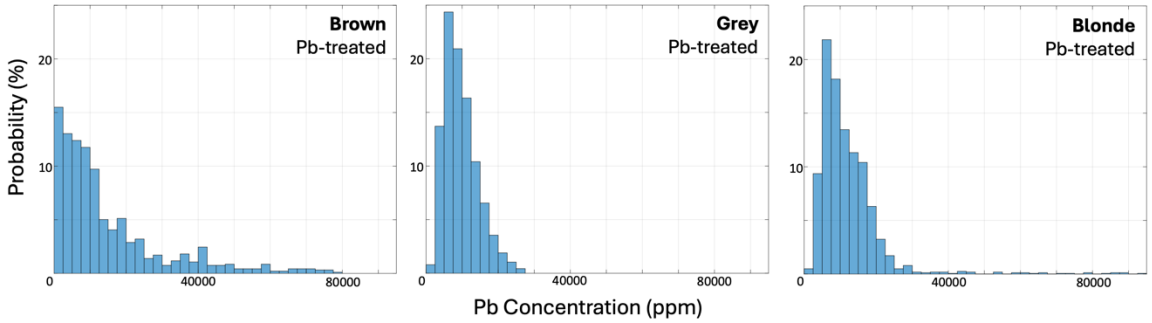

Figure 3.13: Histogram probability distributions of the lead concentration for each pixel in the fine scans of lead-treated human hair samples from figure 3.11. Lead concentrations for each pixel were calculated using a beam flux of 3.73 x 10^8 photons/s.

Grey and blonde hair samples display a single distinct peak in the distribution, occurring in the 5000-10000 ppm bin. The distribution for brown hair does not have a a single sharp peak but instead shows that many pixels have low lead content. In the brown hair sample, more pixels correspond to higher lead concentrations than in the grey and blonde samples.

The remaining portions of the hair samples which were not embedded in resin for synchrotron imaging were sent for ICP-MS analysis of total lead content, with the results listed in table 3.3.

Table 3.3: ICP-MS results for total lead content analysis in washed free human hair samples that were either left untreated or were treated with a lead solution.

Sample #	Colour	Lead content (ppm)	
		Untreated (DL: 0.05)	Treated (DL: 20-50)
1	Brown	3.16	24300
6	Grey	24	19700
10	Blonde	68.2	28200

The control samples show that there were extremely low levels of lead in the hair prior to lead treatment, thus the lead detected in the treated samples can be attributed to the biosorption of the lead solution. For the lead-treated samples, the ICP-MS results show that the lead content is lowest for grey hair and highest for blonde hair. The μXRF concentrations maps for lead-treated samples also show that the lead content is lowest for grey hair, but highest for brown hair. The μXRF lead concentration maps for hair samples consistently produced average lead concentrations that were approximately half the values obtained from ICP-MS analysis. A linear regression applied to the results of the lead-treated hair samples shows good correlation between the μXRF and ICP-MS results with a slope of 0.4962 and an R^2 of 0.9509.

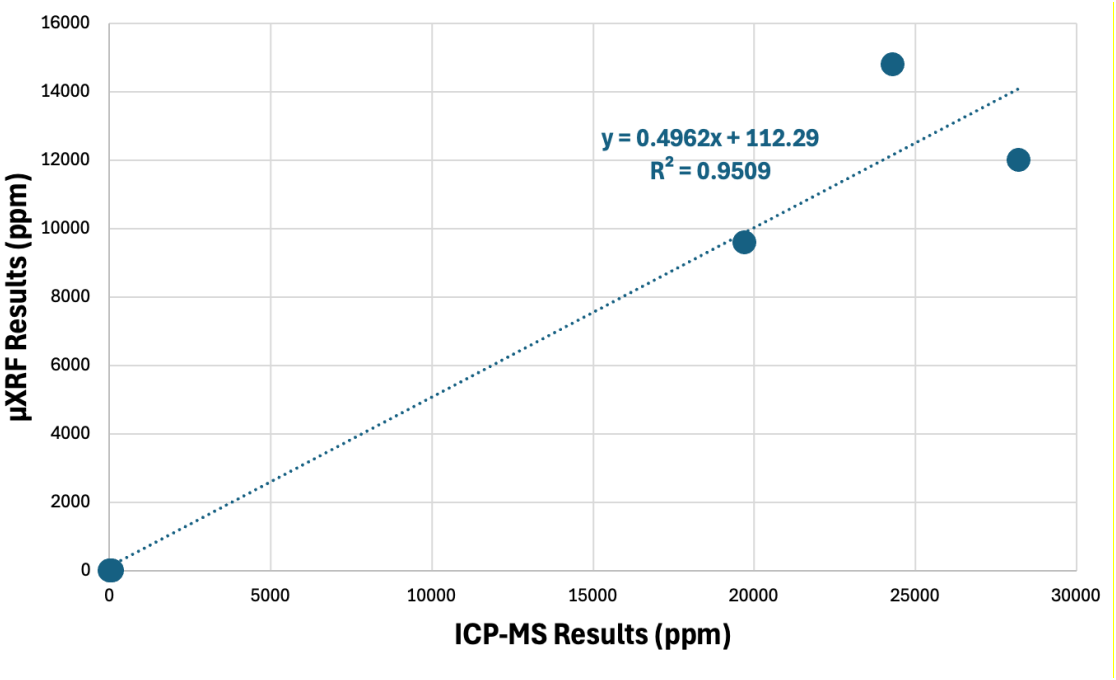

Figure 3.14: Linear regression for µXRF and ICP-MS results of lead content in human hair samples that were either untreated or treated with a lead solution, then embedded in resin. The plotted µXRF results were computed using a flux of 3.73×10^8 photons/s in the PyMCA analysis.

Although the correlation is good ($R^2 = 0.9509$, $p = 0.0009$), the slope is different from 1 by a factor of approximately 0.5.

4 Discussion

4.1 Receptor Solution ICP-MS

It is often hypothesized that the diffusion of substances through the skin is assisted by accessory structures in the skin such as hair follicles and sweat glands [2, 7, 14, 15, 17]. Therefore, it would be expected that the lead solution would pass through the hairy skin more quickly than for skin with no hair and accumulate in the receptor solution following diffusion, resulting in higher levels of lead detected. ICP-MS analysis of the receptor solution following lead diffusion through hairy and hairless skin revealed that the lead content of the receptor solution was consistently lower for hairy skin compared to hairless skin. This suggests that instead of passing through the skin layers, the applied lead acetate is perhaps being bound to the external hair and thus is not available for diffusion into skin, or is accumulating in structures beneath the skin surface which are only present when hair is also present in the skin. It may also suggest that sebum in the hair shaft prevents diffusion. This binding or accumulation is likely to be to or within structures with high sulfide and sulfhydryl groups contents, such as keratin, since lead is known to have a high binding affinity to sulfhydryl groups [21]. Such structures include hair itself, and keratinocytes, which are layered throughout the epidermis [12, 17]. Sebum is a lipid-rich substance, and so lead acetate is unlikely to diffuse well through this material.

The determination of the K_p of lead is important to understanding the risks associated with cutaneous lead application. From the data collected for this thesis, the K_p, a descriptive parameter for the rate of passage of a substance through the skin, could not be

calculated for skin with hair since the diffusion curve either had too much variance or had not reached a point where the linear behaviour of diffusion was observed. It would be expected that the ICP-MS results would show a trend of increasing lead content in the receptor solution as time increases, as previously shown for hairless skin [80]. However, the results show that a greater amount of the applied lead solution passes through hairy skin at 48 hours than at either 24 or 72 hours.

The average lead content of the 24-hour diffusion of lead through hairless skin was calculated from three different experimental trials, each resulting in three receptor solution samples. The spread in the ICP-MS results for these samples is very large, since one of the trials yielded consistent lead concentrations on the order of 10^{-2} ppm, while all other trials yielded consistent lead concentrations on the order of 10^{2} ppm.

The spread of the ICP-MS results is also very large for the 48-hour hairy skin receptor solution samples, with three of the four samples yielding a lead concentration on the order of 10^{2} ppm, and one sample with a lead concentration on the order of 10^{-1} ppm. Since the plotted data from each diffusion time for hairy skin only included four samples from single experimental trials, reproducibility of these results has not yet been shown.

Although the differences in receptor solution lead content were statistically significant ($p < 0.0125$ for 24 hours; $p < 0.03$ for 48 hours; $p < 0.03$ for 72 hours), the sample sizes were very small ($n = 3$-9). More diffusion data is required to strengthen the significance of the results. As data collection is ongoing, more experimental trials will allow precise conclusions to be drawn regarding the diffusion of lead through hairy skin at 24, 48

and 72 hours, and a K_p may potentially be calculated if additional experiments reveal that the lead diffusion through hairy skin at 48 hours presented here represents outlier data and the diffusion does indeed follow the expected trend.

4.2 Skin μXRF

The ability to image the biodistribution of lead in the skin after cutaneous exposure bridges the gap in knowledge between how much lead passes all the way through the skin layers and what path the lead takes to arrive at the hypodermis. The presented data is the first to provide visual evidence of the path of lead through hairy skin using synchrotron μXRF. This is important because it shows that lead is absorbed very quickly into the skin, so even short exposures of a few minutes will result in uptake into skin. Further, it provides evidence to support banning the use of lead acetate as a hair colourant and may guide future directions for studies of uptake of products used specifically in areas of high follicular infundibula volume such as the forehead and sural region [30].

In figures 3.3 and 3.4, it is evident that lead is able to permeate through the stratum corneum within 30 minutes of application to a depth greater than the stratum corneum, with differential lead diffusion depths in relation to the hair below the skin surface seen at short diffusion times. As predicted by Fick's first law of diffusion, the lead is diffusing along a concentration gradient from high to low concentration, thus, the lead content near the application site on the skin surface is much higher and decreases as the depth into the skin increases [19]. For the second sample imaged for the 24-hour diffusion experiment, lead

uptake is seen in small clusters in the skin surface, within the hair protruding from the skin surface, and near the hair follicle below the skin surface. As mentioned in section 1.2, keratinocytes are densely populated in the epidermis and secrete melanin [17]. Keratin and melanin are good candidates for metal binding by the presence of sulfhydryl groups and through ionic interactions, respectively, and are also both present in the hair shaft and follicle [21]. For long diffusion times, the lead is also seen to collect on the edges of the hair pore, possibly due to the expected attraction of lead to the sulfhydryl groups located in the hair shaft. The distribution of lead in the skin with hair may be affected by this, as the keratinocyte distribution in hairless skin appears uniform while the keratinocyte distribution varies in hairy skin. Repulsion by sebum may also be a factor contributing to patterns of lead diffusion away from the underlying hair shaft and along the hair pore.

Hairy skin control samples which were left unexposed to the Franz diffusion cells and unexposed to lead resulted in ICP-MS-detected lead content below the detection limit (40 ppm) for small (0.13 g) skin samples, and average μXRF lead concentrations between 230-330 ppm. As previously mentioned, some buildings constructed prior to 1980 have shown evidence of house dust levels of approximately 450 ppm [61]. While the μXRF-derived lead concentrations in control skin samples are non-zero, the building in which experimental skin was prepared was constructed in 1968, thus the lead content of the control samples falls below the level of lead expected in the dust of the experimental environment. This shows that the level of caution taken to avoid contamination of experimental samples, including the usage of a HEPA-filtered biosafety cabinet in a HEPA-filtered clean room for lead exposure experiments, limits exogenous lead contamination

that is otherwise unavoidable due to the ubiquity of lead in the environment. This limits the number of factors contributing to experimental uncertainty, and allows experimental diffusion results to come solely from the diffusion of the applied lead.

Synchrotron μXRF is often used for qualitative analysis with the goal to understand the distribution and relative elemental concentrations for the element of interest based on pixel intensity. The quantitative analysis applied here aims to use PyMCA to produce an accurate elemental concentration distribution, with verification by comparison to ICP-MS results. This quantitative analysis became an iterative approach as lead concentration outputs were much larger than expected when the beam flux determined using the NIST 610 standard was used. Since the whole sample is acid-digested during ICP-MS analysis, the results from ICP-MS of the skin were compared to the average calculated lead concentrations resulting from μXRF data. Overall, the μXRF-derived results from a beam flux found using the NIST 610 standard reference material were highly correlated and within a factor of 4 of the ICP-MS data, which is quite close in terms of absolute quantification of μXRF maps. This suggests that the quantitative results obtained are a factor of 4 too high. There is likely a multiplying factor missing from some point in the PyMCA analysis, however despite thorough review of the parameters of the experimental set-up and consultation with beam line scientists in France and Canada, this factor has not yet been identified. Another possible reason for differences between the ICP-MS and μXRF-derived results for lead quantification could come from the fact that the μXRF imaging of tissue sections only measures a 25 μm thick slice of the skin, thus any regional

variation in lead diffusion across the larger skin sample sent for ICP-MS analysis would be missing from μXRF imaging results.

Quantitatively, the average lead concentrations in skin found from the coarse scans (figure 3.3) consistently provided lead concentrations which were very similar to the fine scan (figure 3.4) outputs of matched samples, with the highest variation of 27% occurring for one of the 24-hour samples. Both PyMCA analyses of coarse and fine scans of skin used the a flux of 3.73×10^8 photons/s, only changing the dwell time to account for the difference in acquisition parameters. This suggests that for studying the diffusion of lead through the skin, if the beam flux is accurately determined, μXRF data acquired solely for the purpose of quantification can use the lower resolution 20 μm step size with 50 ms dwell time (coarse) imaging as a reliable alternative to fine resolution imaging since the obtained outputs only vary by 11-27% in extreme cases, thus saving beamtime that can be used for more acquisitions. Furthermore, macro-resolution scanning would allow larger areas to be scanned in replicates, allowing a more robust statistical assessment of lead penetration into skin. Although there is some degree of discrepancy in the quantification output of the two methods used, these results still provide valuable information about the behaviour of lead diffusion through hairy skin.

Probability distributions of the lead concentration in each μXRF image pixel often show a single distinct peak, followed by an exponential decrease in probability for pixels of higher lead concentrations. The peaks in the distribution may show some biological phenomena related to the structures underlying the skin surface, such as the number of keratinocytes present in the skin sample. The probability histograms were constructed

solely from data within the defined skin region of the images, however there are large gaps in the skin of the 2- and 24-hour samples resulting from the sample preparation process, easily seen in the microscope images in figure 3.4. This could be causing the peaks of those distributions to be shifted to the left of the peak value for the 0.5- and 1-hour samples. The largest gap appears on the 2-hour sample, which could be causing the distribution to have a linearly decreasing shape as lead concentration increases. On the contrary, the 24-hour samples both have regions where the sample has folded over itself, causing lead concentrations in those regions to be higher than expected. This could cause of the presence of pixels with lead concentrations above 1000000 ppm, which are not usually present in the samples with shorter diffusion times, however ICP-MS results support that the distribution would include more pixels with higher lead concentration with increasing diffusion time.

The diffusion of lead through the skin directly above the hair follicle appears to be impacted, which is especially noticeable for diffusion times less than 2 hours in figure 3.4. To investigate these differences, lead diffusion profiles from the skin surface towards the subcutaneous layers at various locations relative to the location of the underlying hair follicle were investigated for the 1-hour lead diffusion sample. This specific sample was selected since the literature suggests that differences in skin diffusion attributed to the presence of hair should be observed within the first 30 minutes of diffusion, and because the differences in lead diffusion depth related to the position of the hair follicle were most evident for this sample [64]. In addition, this analysis was applied to the fine scan to ensure subtle details in the diffusion profiles were detected, and the fine scan for the 0.5-hour

sample did not include enough image data for a diffusion profile from the skin surface to the centroid of the underlying hair. The differences in lead diffusion at different positions on the skin surface relative to the underlying hair were statistically significant, with deeper diffusion occurring further from the follicle. This suggests that the structures and substances around hair, such as apocrine sweat or sebum, may repel the dissolved lead ions within the skin, which contradicts hypotheses that the lead would be attracted to the sulfhydryl groups of the hair due to their binding affinities. More μXRF images should be acquired for hairy skin samples with short diffusion times to fully understand the differences in diffusion related to the hair.

4.3 Skin XAS

As mentioned, lead (II) acetate dissolved in water was applied to the skin surface for diffusion. Lead (II) acetate contains divalent lead, thus reference spectra for compounds containing tetravalent lead are unlikely components in the LCF results for sample spectra. Despite this, the results from XANES measurements often yield LCF including standards composed of tetravalent lead in addition to divalent lead compounds.

From the LCF results, lead (II) acetate contributes to twelve of the sixteen LCF to the acquired XANES for the 24-hour diffusion samples. This is expected since lead (II) acetate trihydrate was applied to the skin and is water-soluble. Moreover, it was proposed by Bos and Meinardi that the molecular weight limit for chemical compounds to be absorbed rapidly through the skin is 500 Da [81]. Lead (II) acetate trihydrate has a molar

mass of 379.3 g/mol or 379.3 Da, which is smaller than the 500 Da limit, and therefore the lead (II) acetate trihydrate molecule should be able to penetrate the skin if not fully dissolved into its respective ions. Soluble lead acetate can also react with a variety of substances to form various compounds, such as inorganic $PbCO_3$, which is also a common contributor to the LCF results. $PbCO_3$ could be formed from reactions with carbon dioxide in the skin and is present in most LCF results corresponding to XANES measured along the hair shaft [82]. The presence of water-insoluble $PbCO_3$ along the hair shaft is probable since the keratinized cells of the hair matrix are also relatively water-insoluble [36]. $PbCl_2$ could also be formed from lead acetate from reactions with sodium and potassium salts (NaCl and KCl) found in various layers of the epidermis, resulting in the formation of ionic compounds between lead and chloride ions [16]. The coincidence of $PbCO_3$ and $PbCl_2$ in samples is interesting and may imply the occurrence of various reactions within the skin and hair. It is possible for $PbCO_3$ to be involved in a chain of reactions leading to the formation of $PbCl_2$, however this reaction would be highly unlikely since it would involve the presence of nitric acid, which is highly corrosive [83].

Table 3.2 also reveals that tetravalent lead compounds have also been incorporated into the LCF results. As mentioned in section 3.3.3, PbO is the most common tetravalent lead compound contributing to the LCF in for the first 24-hour diffusion sample, while PbO_2 is the most common tetravalent lead compound found in the LCF for the second 24-hour diffusion sample. Most XANES for the first 24-hour diffusion sample were acquired in regions beneath the skin surface, while many XANES for the second 24-hour diffusion sample were along the exposed and underlying hair shaft. This could indicate the presence

of lead compounds of similar structure to PbO beneath and throughout the skin, or lead compounds of similar structure to PbO_2 along the hair shaft.

As seen in figure 3.2 which depicts the XANES spectra for reference lead compounds, tetravalent lead has a characteristic pre-edge feature corresponding to the 2p → 6s transition which is not possible for divalent lead [84]. Pb_3O_4 can be formed with either divalent or tetravalent lead, therefore it cannot be disqualified as a component as easily, however from visualization of the Pb_3O_4 reference spectra, the reference material appears to have the distinct 2p → 6s transition peak as observed with PbO and PbO_2. Divalent Pb_3O_4 should be investigated in the future to verify the formation of this compound within the skin. LCF results which include the tetravalent compounds may indicate changes in the local environment unrelated to the formation of these compounds, or possibly other biologically relevant lead compounds have been formed which have similar local or electronic coordination, and thus similar XANES spectra to these compounds. For example, studies of the interactions between lead (II) and cysteine residues by Jalilehvand et al. have found that lead (II) is likely to have a tetrahedral configuration to four sulfur donor atoms, which is one of the possible geometries for Pb_3O_4 [85].

Comparing the spectra of reference tetravalent lead compounds directly to the sample measurements, it is clear that tetravalent lead compounds, including PbO and PbO_2 can be eliminated as possible candidates for forms of lead within the sample. When finding the best LCF to the data, the Larch program provides multiple LCF results in which the component weights vary, with results listed from best to worst based on lowest χ^2 value. To understand the inclusion of tetravalent compounds into the LCF, a sample measurement

whose three best LCF results include different combinations of tetravalent lead compounds (acquisition 10) was compared individually to the reference compounds contributing to the fits.

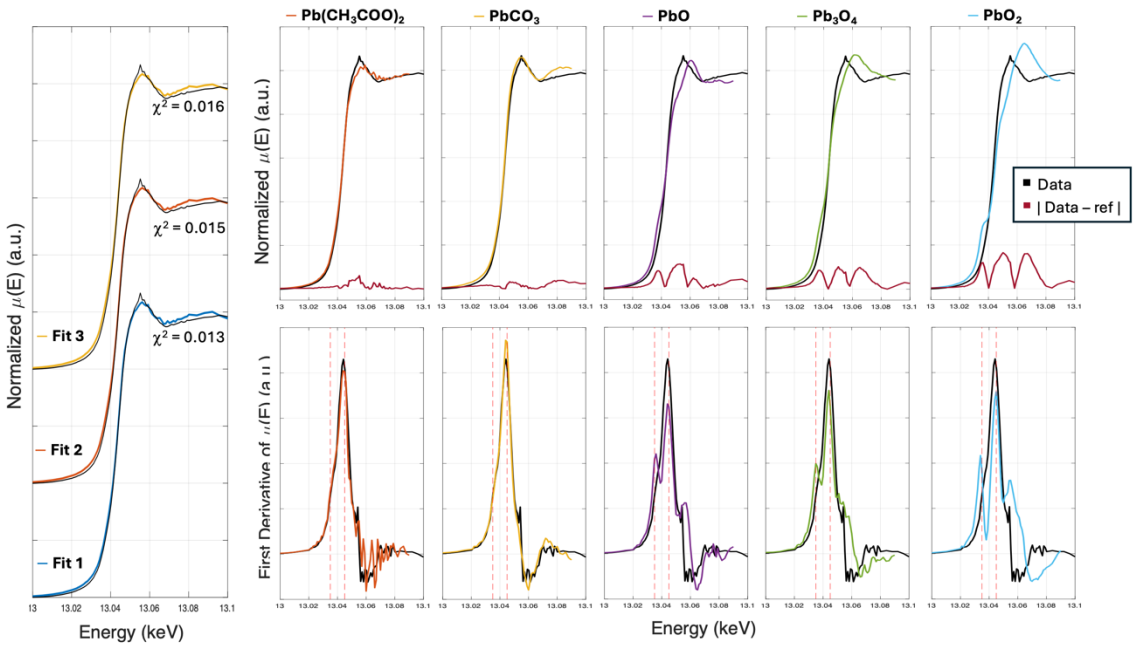

Figure 4.1: Three best LCF results for XANES measurement 10 which contain: lead acetate and $PbCO_3$ (fit 1, χ^2 = 0.013); PbO, PbO_2, lead acetate, Pb_3O_4, and $PbCO_3$ (fit 2, χ^2 = 0.015); PbO, lead acetate, Pb_3O_4 and $PbCO_3$ (fit 3, χ^2 = 0.016). The XANES measurement is compared individually to each reference spectra included in the LCF combinations to determine which compounds should be included in the true LCF.

From figure 4.1, it is evident that PbO, PbO_2 and Pb_3O_4 should not be included in the best fit. The tetravalent reference XANES spectra show large differences from the sample measurement around the edge and peak in the plots of the normalized μ(E) vs. beam energy, while lead acetate and $PbCO_3$ display relatively low deviations from the measurement

spectrum. Additionally, the first derivative plots show the absence of the 2p → 6s transition in the sample measurement, which is present for the tetravalent PbO, PbO_2 and Pb_3O_4 compounds. This only leaves fit 1 as a candidate for the true best fit to the measurement, since it is the only LCF that does not include these tetravalent lead compounds. Similar results were obtained for other XANES measurements with tetravalent lead compounds contributing to the LCF.

Furthermore, the LCF model does not perform well when tetravalent lead compounds are included in the LCF result. In the four cases where the LCF component weights summed to values above or below 100%, PbO was the only compound listed as a contributor to the LCF for every case. Since this compound is not likely to be present in the XANES measurement locations, its inclusion could be disrupting the LCF model.

It was hypothesized that the high sulfur content of hair would give rise to the formation of lead-sulfur compounds, especially since lead has a high affinity for binding to sulfhydryl side chains of amino acids [21]. In addition, hydrogen sulfide (H_2S) which is known to be produced in the skin, can react with lead (II) ions in lead acetate to form insoluble lead (II) sulfide (PbS) [86, 87]. Since there were no reference spectra which included sulfur, this cannot be confirmed or denied, however speculations regarding similarities in local geometry and electronic configuration may hint at whether or not it is present in the sample at the sampled points.

4.4 Hair μXRF

The absorption of lead acetate into the hair shaft was of interest for this study to support μXRF and ICP-MS findings of the diffusion of lead into hairy skin. Free human hair cross sections embedded in resin were imaged using synchrotron μXRF under fine scan conditions at a sample-to-detector distance of 3.5 cm. These parameters were used to account for the small size of the hair cross sections (diameter 45-110 μm) and to reduce the attenuation of low lead signals through the air prior to reaching the detector, respectively [28].

As mentioned by da França et al., hair dye molecules enter the hair matrix by first passing through non-keratinized regions associated with low levels of sulfur-containing amino acids, then subsequently migrate to keratinized regions where they become incorporated into the hair matrix [12]. μXRF data indicates specific lead uptake in the cuticle, with equally or less intense lead uptake in the medulla. Both the cuticle and medulla of the hair are considered keratinized, where keratins rich in sulfur-containing amino acids are available for lead to bind. Human hair may or may not be medullated along the length of the hair, however there is evidence here that when the hair is medullated, lead uptake is possible in this region. Microscope images of human hair cross sections from the same subject prove that medullation along the hair shaft and across different strands of hair from the same source vary in medullation [88].

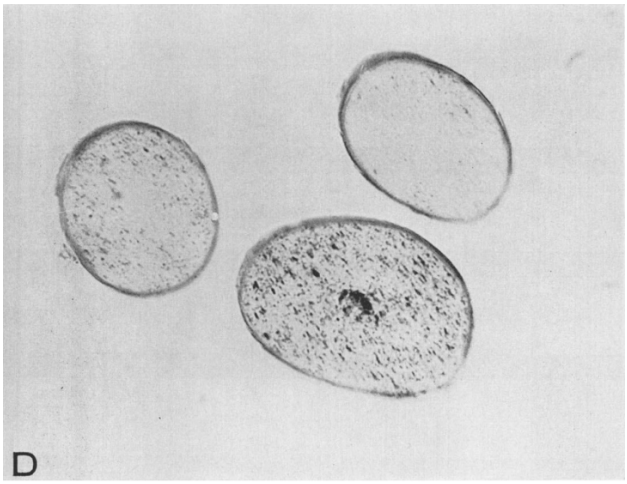

Figure 4.2: Microscope image of brown and grey hair cross sections from the same source [88]. Hair cross sections vary in size, shape, and medullation.

It is also observed that lead does not accumulate to a high degree in the cortex, which agrees with the anatomy of this region being considered non-keratinized and thus having lower sulfur levels for lead binding. Extremely low levels of lead were detected in this region compared to the cuticle and medulla, likely related to the rate of lead passage from the cuticle into the medulla via the cortex.

Without ICP-MS or μXRF results for the unwashed, untreated hair samples, it is difficult to tell whether the hair cleaning procedure was successful in removing exogenous lead contamination. However, there were very low levels of lead detected from both the ICP-MS and μXRF analyses for the washed, untreated hair samples, where ICP-MS results were comparable to or less than Canadian urban background house dust levels [77].

Taking the regions of lead accumulation observed for the human hair shaft into account, the variation in hair medullation and selective lead uptake in the cuticle is also

seen in the μXRF images of the 24-hour diffusion of lead acetate through hairy skin, especially in figure 3.4. In the portion of the hair protruding from the skin surface, lead is detected along the cuticle and within the medulla of hair shaft. Although there appears to be lead uptake in the cortex as well, this region of uptake is likely only occurring in the medulla which occupies a larger area of the overall hair shaft diameter in lower animals (>1/3) compared to human hair (<1/3), leaving the hair cortex thinner for lower animals than for humans [27]. In the portion of the hair shaft that would have been beneath the skin, lead only accumulates along the cuticle. This could be due to discontinuities in the medulla in the hair shaft beneath the skin surface, however the medulla of lower animals is usually continuous and regularly structured [27].

The beam flux used for quantitative analysis of the human hair samples was found from a linear regression comparing the μXRF lead concentration outputs to the results obtained from ICP-MS analysis of human hair samples from the same batch. The beam flux found from the NIST 610 standard was used for the initial comparison, where it was found that the μXRF results were correlated to the ICP-MS results within a factor of 0.5. Various factors may play a role in this discrepancy, such as differences in the hair morphology along the length of the hair shaft and thus differences in lead absorption along the hair shaft. Differences in lead uptake depending on hair colour from ICP-MS results suggests that lead could be more likely to bind to pheomelanin than eumelanin. This is supported by the results of elemental analysis conducted by Prota where pheomelanin was found to have much higher sulfur content than eumelanin [89]. The discrepancy between the μXRF and ICP-MS results for lead content in the free hair samples is also interesting since it is 8 times

smaller than the discrepancy found between the μXRF and ICP-MS results for the hairy skin samples. One of the biggest differences between the acquisitions for hairy skin and free hair samples was the distance from the sample to the detector, where the sample was approximately 8 cm from the detector for hairy skin and approximately 3.5 cm from the detector for free hair samples. Because μXRF data for the NIST 610 standard was only collected at a sample-to-detector distance of 8 cm, the μXRF-derived results for lead quantification in the free hair samples are more likely to be inaccurate. For data collection of both the standard and sample, the experimental configuration and detector set-up must be the same. This could be another factor leading to the difference in linear regression results for μXRF comparisons to ICP-MS results for skin and for hair. This result provides evidence of factors potentially missing from or incorrectly calculated in the PyMCA analysis, possibly related to the PyMCA calculations using the fundamental parameters approach.

There may be a small dependence on the portion of the hair shaft used for each analysis since the hair matrix, and thus the ability for biosorption, varies along the length of the hair shaft [78]. The greater portion used for ICP-MS may have been dominated by sulfhydryl groups, increased in pigmentation and thus melanin content along the length of the hair, or due to the amorphous nature of the human hair medulla, the medulla may have been thicker in this portion of the hair shaft and taken up more lead than in the section used for μXRF. Because the portion of the hair used for μXRF imaging was only 10 μm thick, it limits the ability to make conclusions about the lead uptake along the entire hair shaft. In

the future, hair cross sections in the longitudinal direction should be attempted to gain a better idea of lead absorption along the length of the hair.

Since this study was a first look at the absorption of lead acetate into the hair shaft, a simple solution of lead acetate dissolved in deionized water was used for the lead treatment. A visible colour change of the hair shaft was not noted here, likely due to the lack of sulfides and oxidizing components in the prepared lead solution. According to Mast, sulfides are required for hair dyes using lead acetate as the colourant to work effectively [60]. Since this study has shown the ability of lead acetate dissolved in water to be absorbed by the hair shaft, future studies using lead acetate solutions should incorporate sulfides and/or oxidizing agents to test the role these components play in the absorption of lead into the hair shaft.

4.5 Challenges

While the Franz cell diffusion technique has been well established, our group is the first, to our knowledge, to use synchrotron μXRF to determine the elemental lead in the skin and subsequently the lead concentration throughout the sample. The first challenge with the use of synchrotron techniques is that there is generally a limited allotted beamtime. Although a number of μXRF images were acquired for this project, it is difficult to make conclusions about the behaviour of lead diffusion since there was not enough time to acquire images for multiple different samples from each diffusion time. Further measurements should also be made during a future beam time for diffusion times between

2 and 24 hours to better understand the pattern of diffusion as the lead is absorbed further into the skin and around the hair follicle.

In addition, the determination of the beam flux was challenging as the beam flux predicted for analysis of skin using the NIST 610 standard reference material was much lower than expected. Various PyMCA analyses were completed for multiple beam fluxes, sometimes yielding mass fractions of lead which were much higher than expected. ICP-MS results along with comparisons of the lead mass fractions for fine and coarse scans of the same sample were essential in guiding beam flux decisions. Going forward, the standard should consist of a thin, evenly coated layer of pure lead at concentrations relevant to the studied biological system. Furthermore, data collection for the standard must be performed under the same conditions and parameters as the samples. These considerations along with comparisons to ICP-MS results should be implemented to ensure more accurate calibration for determining the flux and quantifying lead in the samples.

The density used for the sample matrix in the PyMCA analysis was found to have effects on the lead concentration outputs from PyMCA. Changing the density of the skin matrix by 0.05 g/cm^3 can cause differences in lead concentration outputs by two orders of magnitude. This may suggest that the analyses of the fat and skin layers should be completed separately to ensure the correct density for each tissue is used to obtain more accurate results.

5 Summary, Conclusions and Future Work

While there has been prior work showing lead acetate diffuses through skin, this thesis work has shown that lead (II) acetate can diffuse through hairy skin, supported by ICP-MS analysis of Franz diffusion cell receptor solution. Most importantly, this work has shown that it is feasible to visualize the spatial distribution of absorbed lead in hairy skin by synchrotron μXRF. Through synchrotron XAS measurements, this work has found that lead (II) acetate persists through the skin as the lead diffuses towards the subcutaneous layers, with highly probable formation of $PbCO_3$ and $PbCl_2$ at sites within the skin. These findings suggest that current practices for lead safety must be improved, as lead levels within the skin and the levels passing through the skin are higher than previously understood, although the exact mechanism of lead diffusion and accumulation in skin is not yet fully understood.

The work of this thesis has produced results from both ICP-MS analysis and qualitative μXRF imaging that suggest that the presence of hair protruding from and underlying the skin does not increase the absorption of lead through the skin. This finding is counter to the common hypothesis that hair follicles increase absorption through the skin. ICP-MS data showed no increase in absorption with some suggestion of a decrease. μXRF images showed that the diffusion of lead was reduced at the skin surface above hairs, especially at short diffusion times. To fully understand which skin structures are affecting the pathway of lead absorption into the skin, a side-by-side comparison with stained skin sections would be useful. While this data is preliminary, this is a result that is worth exploring further.

While quantification was achieved through comparison with ICP-MS, direct quantification from synchrotron techniques should be improved. The levels predicted using PyMCA were a factor of 4 high for skin and a factor of 2 low for hair, and the factors leading to this difference were not determined by the time of writing this thesis. For the μXRF analysis, the fundamental parameter model must be calibrated using a thin, homogeneously distributed standard only containing lead at a concentration relevant to the biological system under investigation (e.g. a sputtered lead standard). In addition, all datasets, including the standard, should be collected under the same experimental configuration. With an accurately determined flux, the resulting lead concentration distribution maps could provide direct outputs which are comparable to the ICP-MS results, without the requirement of a separate ICP-MS validation for each set of beam time measurements.

The work in this thesis has shown that XAS is a viable technique for studying the form of lead as it passes through the skin. It was found that some lead did change form as it passed through the skin, although in the majority of the points in the skin, the major form of lead was still lead acetate. While it has been shown worthwhile, the XAS LCF analysis will be improved by increasing the library of lead reference compounds to include more physiologically relevant compounds, such as $Pb_3(PO_4)_2$, $PbSO_4$, and PbS. The development of new XAS reference standards should be a priority.

Overall, this project has proved the feasibility of using a synchrotron source to image the path and form of lead through hairy skin, which has not been shown to date, to our knowledge. The mass fractions calculated from μXRF maps, when compared to ICP-

MS data show that this approach does provide quantification to within a factor of 4. In addition, this work showed the feasibility of measuring changes in lead compounds as the lead is absorbed into the skin. With further refinement in the sample preparation, this method for the determination of the spatial distribution and form of lead in hairy skin will be useful for future experiments studying the percutaneous diffusion of other relevant lead compounds found in cosmetics. Such lead compounds include lead sulfide, which has been incorporated into kohl eyeliners which are applied next to eyelashes, and lead tetroxide, which has been found in culturally significant cosmetics such as sindoor and henna which are both applied to the hair [90].

6 References

[1] D. R. Smith, J. D. Osterloh, S. Niemeyer, and A. R. Flegal, "Stable Isotope Labelling of Lead Compartments in Rats with Ultralow Lead Concentrations," *Environmental Research*, vol. 57, pp. 190-207, 1992.

[2] R. T. Niemeier, A. Maier, and J. F. Reichard, "Rapid Review of Dermal Penetration and Absorption of Inorganic Lead Compounds for Occupational Risk Assessment," *Annals of Work Exposures and Health*, vol. 66, no. 3, pp. 291-311, 2022.

[3] L. Järup, "Hazards of heavy metal contamination," *British Medical Bulletin*, vol. 68, no. 1, pp. 167-182, 2003.

[4] S. G. Lilley, T. M. Florence, and J. L. Stauber, "The used of sweat to monitor lead absorption through the skin," *The Science of the Total Environment*, vol. 76, pp. 267-278, 1988.

[5] O. E. Orisakwe and J. O. Otaraku, "Metal Concentrations in Cosmetics Commonly Used in Nigeria," *The Scientific World Journal*, vol. 2013, no. 1, 2013.

[6] R. Zhang, L. Li, Y. Sultanbawa, and Z. P. Xu, "X-ray fluorescence imaging of metals and metalloids in biological systems," *Am J Nucl Med Mol Imaging*, vol. 8, no. 3, pp. 169-188, 2018.

[7] J. L. Stauber, T. M. Florence, B. L. Gulson, and L. S. Dale, "Percutaneous absorption of inorganic lead compounds," *The Science of the Total Environment*, vol. 145, pp. 55-70, 1994.

[8] B. R. Allen, M. R. Moore, and J. A. A. Hunter, "Lead and the skin," *British Journal of Dermatology*, vol. 92, no. 6, pp. 715-719, 1975.

[9] J. A. Witkowski and L. C. Parish, "You've Come a Long Way Baby: A History of Cosmetic Lead Toxicity," *Clinics in Dermatology*, vol. 19, pp. 367-370, 2001.

[10] L. A. Sayre, Three Case of Lead Palsy from the use of a Cosmetic called "Laird's Bloom of Youth." Philadelphia: Collins, printer, 1869.

[11] U. S. Food and Drug Administration. "Limiting Lead in Lipstick and Other Cosmetics." fda.gov. Accessed: Oct. 25, 2024. [Online] Available: https://www.fda.gov/cosmetics/cosmetic-products/limiting-lead-lipstick-and-other-cosmetics

[12] S. A. da França, M. F. Dario, V. B. Esteves, A. R. Baby, and M. V. R. Velasco, "Types of Hair Dye and Their Mechanisms of Action," *Cosmetics*, vol. 2, pp. 110-126, 2015.

[13] U. S. Food and Drug Administration. "Lead Acetate in "*Progressive*" Hair Dye Products." fda.gov. Accessed: Oct. 25, 2024. [Online]. Available: https://www.fda.gov/cosmetics/cosmetic-products/lead-acetate-progressive-hair-dye-products

[14] M. R. Moore, P. A. Meredith, W. S. Watson, D. J. Sumner, M. K. Taylor, and A. Goldberg, "The percutaneous absorption of lead-203 in humans from cosmetic

preparations containing lead acetate, as assessed by whole-body counting and other techniques," *Fd Cosmet Toxicol.*, vol. 18, pp. 399-405, 1979.

[15] A. Franken, F. C. Eloff, J. Du Plessis, and J. L. Du Plessis, "*In Vitro* Permeation of Metals through Human Skin: A Review and Recommendations," *Chem. Res. Toxicol.*, vol. 28, pp. 2237-2249, 2015.

[16] M. Haftek, R. Abdayem, and P. Guyonnet-Debersac, "Skin Minerals: Key Roles of Inorganic Elements in Skin Physiological Functions," *Int. J. Mol. Sci.*, vol. 23, no. 11, 2022.

[17] F. H. Martini, J. L. Nath, and E. F. Bartholomew, "The Integumentary System," in *Fundamentals of Anatomy & Physiology, Global Edition, 11th ed.*, Boston: Pearson Education, 2018, ch. 5, pp. 198-225.

[18] D. R. Friend, "In vitro skin permeation techniques," *Journal of Controlled Release*, vol. 18, pp. 235-248, 1992.

[19] S. Mitragotri, *et al.*, "Mathematical models of skin permeability: An overview," *International Journal of Pharmaceutics*, vol. 418, pp. 115-129, 2011.

[20] H. Gray, *Gray's Anatomy: With original illustrations by Henry Carter*, London, England: Arcturus Publishing Ltd, 2015.

[21] D. Pozebon, G. L. Scheffler, and V. L. Dressler, "Elemental hair analysis: A review of procedures and applications," *Analytica Chimica Acta*, vol. 992, 2017.

[22] D. L. Wong, M. E. Merrifield-MacRae, and M. J. Stillman, "Lead(II) Binding in Metallothioneins," *Metal Ions in Life Sciences,* vol. 17, pp. 241-269, 2017.

[23] W. C. Bress and J. H. Bidanset, "Percutaneous in vivo and in vitro absorption of lead," *Veterinary and Human Toxicology,* vol. 33, no. 3, pp. 212-214, 1991.

[24] M. E. Herbig, *et al.*, "A custom tailored model to investigate skin penetration in porcine skin and its comparison with human skin," *European Journal of Pharmaceutics and Biopharmaceutics*, vol. 95, pp. 99-109, 2015.

[25] S. Debeer, *et al.*, "Comparative histology and immunohistochemistry of porcine versus human skin," *Eur J Dermatol*, vol. 23, no. 4, pp. 456-466, 2013.

[26] L. B. Baker, "Physiology of sweat gland function: The roles of sweating and sweat composition in human health," *Temperature*, vol. 6, no. 3, pp. 211-259, 2019.

[27] J. W. Hicks, "Microscopy of Hairs; A Practical Guide and Manual," *Federal Bureau of Investigation U.S. Department of Justice*, no. 2, pp. 1-40, 1977.

[28] C. R. Robbins, "Morphological, Macromolecular Structure and Hair Growth," in *Chemical and Physical Behaviour of Human Hair, 5th ed.*, Clermont: Springer, 2012, ch. 1, pp. 6, 76-92.

[29] M. R. Harkey, "Anatomy and physiology of hair," *Forensic Science International*, vol. 53, pp. 9-18, 1993.

[30] B. Buffoli, *et al.*, "The human hair: from anatomy to physiology," *International Journal of Dermatology*, vol. 53, pp. 331-341, 2014.

[31] Y. Jiang, *et al.,* "Atlas of Prenatal Hair Follicle Morphogenesis Using the Pig as a Model System," *Frontiers in Cell and Developmental Biology*, vol. 9, no. 721979, 2021.

[32] J. J. Mayer, "Wild pig physical characteristics," in *Wild pigs: biology, damage, control techniques and management,* South Carolina: Savannah River National Laboratory, United States Department of Energy, 2009, pp. 25-50.

[33] W. Chi, E. Wu, and B. A. Morgan, "Dermal papilla cell number specifies hair size, shape and cycling and its reduction causes follicular decline," *Development*, vol. 140, pp. 1676-1683, 2013.

[34] O. J. X. Morel and R. M. Christie, "Current Trends in the Chemistry of Permanent Hair Dyeing," *Chem. Rev.*, vol. 111, pp. 2537-2561, 2011.

[35] J. F. Corbett, "Hair Coloring," Clinics in Dermatology, vol. 6, 1988, pp. 93-101.

[36] H. Zhang, F. Carrillo-Navarrate, and C. Palet-Ballús, "Human Hair Biogenic Fiber as a Biosorbent of Multiple Heavy Metals from Aqueous Solutions," *Journal of Natural Fibers*, vol. 19, no. 6, pp. 2018-2033, 2022.

[37] M. Kumar, A. Sharma, S. Mahmood, A. Thakur, M. A. Mirza, and A. Bhatia, "Franz diffusion cell and its implication in skin permeation studies," *Journal of Dispersion Science and Technology*, vol. 45, no. 5, 2024.

[38] PermeGear, Inc. "Diffusion testing fundamentals." permegear.com. Accessed: Feb. 28, 2024. [Online]. Available: https://permegear.com/diffusion-101/

[39] Organisation for Economic Co-operation and Development, "Guidance Notes on Dermal Absorption Studies," in *OECD Environment, Health and Safety Publications: Series on Testing & Assessment*, *2nd ed.*, Paris: OECD Publishing, 2011.

[40] Y. G. Anissimov, J. J. Calcutt, and M. S. Roberts, "Mathematical models in percutaneous absorption," in *Percutaneous Absorption, 5th ed.* CRC Press, 2021, ch. 1, pp. 9-52.

[41] E. Mitchell, P. Kuhn, and E. Garman, "Demystifying the synchrotron trip: a first time user's guide," *Structure*, vol. 7, no. 5, 1999.

[42] M. L. Baker, M. W. Mara, J. J. Yan, K. O. Hodgson, B. Hedman, and E. I. Solomon, "K- and L-edge X-ray Absorption Spectroscopy (XAS) and Resonant Inelastic X-ray Scattering (RIXS) Determination of Differential Orbital Covalency (DOC) of Transition Metal Sites," *Coord Chem Rev*., vol. 345, pp. 182-208, 2017.

[43] F. Adams, "Synchrotron X-ray fluorescence analysis in environmental and earth sciences," *EPJ Web of Conferences*, vol. 9, pp. 165-180, 2010.

[44] H. Shehab, *et al.*, "Feasibility of measuring arsenic and selenium in human skin using *in vivo* x-ray fluorescence (XRF) – a comparison of methods," *Physiol. Meas.*, vol. 37, pp. 145-161, 2016.

[45] A. Kodre, M. Hribar, B. Ajlec, and J. Pahor, "*L*-Subshell Fluorescence Yields of Lead," *A. Phys. A – Atoms and Nuclei*, vol. 303, pp. 23-26, 1981.

[46] M. J. Farquharson, A. P. Bagshaw, J. B. Porter, and R. D. Abeysinghe, "The use of skin Fe levels as a surrogate marker for organ Fe levels, to monitor treatment in cases of iron overload," *Phys. Med. Biol.*, vol. 45, pp. 1387-1396, 2000.

[47] K. Geraki, M. J. Farquharson, and D. A. Bradley, "Concentrations of Fe, Cu and Zn in breast tissue: a synchrotron XRF study," *Phys. Med. Biol.*, vol. 47, pp. 2327-2339, 2002.

[48] G. E. Falchini, A. Malezan, M. E. Poletti, E. Soria, M. Pasqualini, and R. D. Perez, "Analysis of phosphorus content in cancer tissue by synchrotron micro-XRF," *Radiation Physics and Chemistry*, vol. 179, 2021.

[49] B. De Samber, *et al*., "Three-dimensional elemental imaging by means of synchrotron radiation micro-XRF: developments and applications in environmental chemistry," *Anal Bioanal Chem*, vol. 390, pp. 267-271, 2008.

[50] G. Veronesi, E. Koudouna, M. Cotte, F. L. Martin, and A. J. Quantock, "X-ray absorption near-edge strcutrue (XANES) spectroscopy identifies differential sulfur speciation in corneal tissue," *Anal Bioanal Chem*, vol. 405, pp. 6613-6620, 2013.

[51] A. Al-Ebraheem, *et al.*, "Effect of sample preparation techniques on the concentrations and distributions of elements in biological tissues using μSRXRF: a comparative study," *Physiol. Meas.*, vol. 36, pp. N51-60, 2015.

[52] M. R. Gherase and D. E. B. Fleming, "Probing Trace Elements in Human Tissues with Synchrotron Radiation," *Crystals*, vol. 10, no. 1: 12, 2020.

[53] Y. Chen, *et al.*, "Database of ab initio L-edge X-ray absorption near edge structure," *Scientific Data*, vol. 8, no. 153, 2021.

[54] F. M. F. de Groot, *et al.*, "2p x-ray absorption spectroscopy of 3d transition metal systems," *Journal of Electron Spectroscopy and Related Phenomena*, vol. 249, 2021.

[55] H. S. Kainth and R. Singh, "Chemical shifts of L_3 X-ray absorption edges on lead and thallium compounds by DEXAFS using synchrotron radiation source," *Nuclear Instruments and Methods in Physics Research B*, vol. 407, pp. 197-202, 2017.

[56] G. S. Henderson, F. M. F. de Groot, and B. J. A. Moulton, "X-ray Absorption Near-Edge Structure (XANES) Spectroscopy," *Reviews in Mineralogy & Geochemistry*, vol. 78, pp. 75-138, 2014.

[57] D. Joseph, "Introductory Chapter: Synchrotron Radiation – Basics and Concepts," in *Synchrotron Radiation*, Boston: IntechOpen, 2019, ch. 1, pp. 1-2. Accessed: March, 30, 2025. [Online]. Available: https://www.intechopen.com/chapters/66264.

[58] F. Meirer, *et al.*, "Assessment of chemical species of lead accumulated in tidemarks of human articular cartilage by X-ray absorption near-edge structure," *J. Synchrotron Rad.*, vol. 18, pp. 238-244, 2011.

[59] C. F. Chandler, The American Journal of Pharmacy. Philadelphia: Philadelphia College of Pharmacy, 1907, pp. 362-368.

[60] R. Mast, "Method of coloring hair," European Patent 0294009A1, Dec. 7, 1988.

[61] P. E. Rasmussen, *et al.*, "Canadian House Dust Study: Lead Bioaccessibility and Speciation," *Environ. Sci. Technol.*, vol. 45, pp. 4959-4965, 2011.

[62] V. M. Meidan, M. C. Bonner, and B. B. Michniak, "Transfollicular drug delivery – Is it a reality?" *International Journal of Pharmaceutics*, vol. 306, pp. 1-14, 2005.

[63] L. Bhatia, "X-ray Fluorescence mapping of Pb absorption in pig skin," B.Sc. thesis, Department of Physics and Astronomy, McMaster University, Hamilton, Canada, 2024.

[64] X. Lui, *et al.*, "Hair follicles contribute significantly to penetration through human skin only at times soon after application as a solvent deposited solid in man," *Br J Clin Pharmacol*, vol. 72, no. 5, pp. 768-774, 2011.

[65] Y. Jiang, *et al.*, "Protocol for preparing mammalian skin samples encompassing hair follicles for spatial transcriptomics," *STAR Protocols*, vol. 5., no. 3, 2024.

[66] ProteinTech. "The Complete Guide to Immunohistochemistry." ptglab.com. Accessed: Jun. 3, 2024. Available: https://www.ptglab.com/media/mjopz1mm/ihc-guide_v13_digital.pdf

[67] I. B-A. Razagui, "A Comparative Evaluation of Three Washing Procedures for Minimizing Exogenous Trace Element Contamination in Fetal Scalp Hair of Various Obstetric Outcomes," *Biol Trace Elem Res*, vol. 123, pp. 47-57, 2008.

[68] K. O. Lorentz, *et al.*, "Synchrotron radiation micro X-Ray Fluorescence (SR-μXRF) elemental mapping of ancient hair: Metals and health at 3rd millennium BCE Shahr-I Sokhta, Iran," *Journal of Archaeological Science*, vol. 120, 2020.

[69] S. Schöder, *et al.*, "Heritage research at the PUMA beamline," *Applied Physics A*, vol. 130, no. 848, 2024.

[70] V. A. Solé, E. Papillon, M. Cotte, Ph. Walter, and J. Susini, "A multiplatform code for the analysis of energy-dispersive X-ray fluorescence spectra," *Spectrochimica Acta Part B,* vol. 62, pp. 63-68, 2007.

[71] Stanford Synchrotron Radiation Lightsource, "XAS Powder Sample Weight Calculator." ssrl.slac.stanford.edu. Accessed: Mar. 26, 2024. [Online]. Available: https://www-ssrl.slac.stanford.edu/smbin/mucalwebnew.pl

[72] Certificate of Analysis for NIST Standard Reference Material, 610, National Institute of Standards and Technology, Gaithersburg, USA, April 2012.

[73] K. J. Rao and J. Wong, "A XANES investigation of the bonding of divalent lead in solids," *J. Chem. Phys.*, vol. 81, no. 11, pp. 4832-4843, 1984.

[74] G. P. Williams, "X-ray properties of the elements," in *Center for X-Ray Optics Advanced Light Source: X-Ray Data Booklet, 3rd ed.*, California: Lawrence Berkeley National Laboratory, 2008, pp. 1-6.

[75] National Institute of Standards and Technology. "Composition of SKIN (ICRP)." physics.nist.gov. Accessed: Feb. 1, 2025. [Online]. Available: https://physics.nist.gov/cgi-bin/Star/compos.pl?matno=250

[76] F. E. McNeill, *et al.,* "The decrease in population bone lead levels in Canada between 1993 and 2010 as assessed by in vivo XRF," *Physiol Meas.*, vol. 39, no. 1, 2017.

[77] P. E. Rasmussen, C. Levesque, M. Chénier, H. D. Gardner, H. Jones-Otazo, S. Petrovic, "Canadian House Dust Study: Population-based concentrations, loads and loading rates of arsenic, cadmium, chromium, copper, nickel, lead, and zinc inside urban homes," *Sci Total Environ*., vol. 443, pp. 520-529, 2013.

[78] D. S. H. Funes, K. Bonilla, M. Baudelet, and C. Bridge, "Morphological and chemical profiling for forensic hair examination: A review of quantitative methods," *Forensic Science International*, vol. 346, 2023.

[79] M. Zimmerley, C-Y. Lin, D. C. Oertel, J. M. Marsh, J. L. Ward, and E. O. Potma, "Quantitative detection of chemical compounds in human hair with coherent anti-Stokes Raman scattering microscopy," *J Biomed Opt.*, vol. 14, no. 4, 2009.

[80] T.-L. Pan, P.-W. Wang, S. A. Al-Suwayeh, C.-C. Chen, and J.-Y. Fang, "Skin toxicology of lead species evaluated by their permeability and proteomic profiles: A comparison of organic and inorganic lead," *Toxicology Letters,* vol. 197, no. 1, pp. 19-28, 2010.

[81] J. D. Bos and M. M. H. M. Meinardi, “The 500 Dalton rule for the skin penetration of chemical compounds and drugs,” *Exp Dermatol*, vol. 9, pp. 165-169, 2000.

[82] I. Alkalay, S. Suetsugu, H. Constantine, and M. Stein, “Carbon dioxide elimination across human skin,” *American Journal of Physiology,* vol. 220, no. 5, pp. 1434-1436, 1971.

[83] National Center for Biotechnology Information. “PubChem Compound Summary: Nitric Acid.” pubchem.ncbi.nlm.nih.gov. Accessed: Jun. 25, 2025. [Online], Available: https://pubchem.ncbi.nlm.nih.gov/compound/Nitric-Acid

[84] K. Tanaka, Y. Takahashi, K. Horie, H. Shimizu, and T. Murakami, “Determination of the oxidation state of radiogenic Pb in natural zircon using X-ray absorption near-edge structure,” *Phys Chem Minerals*, vol. 37, no. 4, pp. 249-254, 2010.

[85] F. Jalilehvand, N. S. Sisombath, A. C. Schell, and G. A. Facey, “Lead (II) Complex Formation with *L*-cysteine in Aqueous Solution,” *Inorg Chem.*, vol. 54, no. 5, pp. 2160-2170, 2015.

[86] S. A. Coavoy-Sánchez, S. K. P. Costa, and M. N. Muscará, “Hydrogen sulfide and dermatological diseases,” *Br J Pharmacol*., vol. 177, pp. 857-865, 2020.

[87] Government of Canada. “How to Test For Sulfur in Materials Using Lead Acetate Paper – Canadian Conservation Institute (CCI) Notes 17/5.” canada.ca. Accessed: Jun. 24, 2025. [Online]. Available: https://www.canada.ca/en/conservation-

institute/services/conservation-preservation-publications/canadian-conservation-institute-notes/test-sulfur-acetate-paper.html

[88] W. B. Shelley and S. Öhman, "Technique for cross sectioning hair specimens," *The Journal of Investigative Dermatology*, vol. 52, no. 6, pp. 533-536, 1969.

[89] G. Prota, "Recent Advances in the Chemistry of Melanogenesis in Mammals," *The Journal of Investigative Dermatology,* vol. 75, no. 1, pp. 122-127, 1980.

[90] J. Lewis, "True Colors: Unmasking Hidden Lead in Cosmetics from Low- and Middle-Income Countries," *Environmental Health Perspectives,* vol. 130, no. 4, 2022.